ANL-SMR-18

FY 2014 Sodium-Supercritical CO_2 Interactions in the SNAKE Experiment Facility

Nuclear Engineering Division

About Argonne National Laboratory
Argonne is a U.S. Department of Energy laboratory managed by UChicago Argonne, LLC under contract DE-AC02-06CH11357. The Laboratory's main facility is outside Chicago, at 9700 South Cass Avenue, Argonne, Illinois 60439. For information about Argonne and its pioneering science and technology programs, see www.anl.gov.

DOCUMENT AVAILABILITY

Online Access: U.S. Department of Energy (DOE) reports produced after 1991 and a growing number of pre-1991 documents are available free via DOE's **SciTech Connect** (http://www.osti.gov/scitech/)

Reports not in digital format may be purchased by the public from the National Technical Information Service (NTIS):

U.S. Department of Commerce
National Technical Information Service
5301 Shawnee Rd
Alexandra, VA 22312
www.ntis.gov
Phone: (800) 553-NTIS (6847) or (703) 605-6000
Fax: (703) 605-6900
Email: **orders@ntis.gov**

Reports not in digital format are available to DOE and DOE contractors from the Office of Scientific and Technical Information (OSTI):

U.S. Department of Energy
Office of Scientific and Technical Information
P.O. Box 62
Oak Ridge, TN 37831-0062
www.osti.gov
Phone: (865) 576-8401
Fax: (865) 576-5728
Email: **reports@osti.gov**

Disclaimer
This report was prepared as an account of work sponsored by an agency of the United States Government. Neither the United States Government nor any agency thereof, nor UChicago Argonne, LLC, nor any of their employees or officers, makes any warranty, express or implied, or assumes any legal liability or responsibility for the accuracy, completeness, or usefulness of any information, apparatus, product, or process disclosed, or represents that its use would not infringe privately owned rights. Reference herein to any specific commercial product, process, or service by trade name, trademark, manufacturer, or otherwise, does not necessarily constitute or imply its endorsement, recommendation, or favoring by the United States Government or any agency thereof. The views and opinions of document authors expressed herein do not necessarily state or reflect those of the United States Government or any agency thereof, Argonne National Laboratory, or UChicago Argonne, LLC.

ANL-SMR-18

FY 2014 Sodium-Supercritical CO_2 Interactions in the SNAKE Experiment Facility

prepared by

Craig Gerardi, Nathan Bremer, Stephen Lomperski, James J. Sienicki, and Christopher Grandy

Nuclear Engineering Division

Argonne National Laboratory

September 30, 2014

EXECUTIVE SUMMARY

One appealing feature of the supercritical carbon dioxide Brayton cycle energy conversion system is the small footprint that the hardware requires, which is in part due to the use of compact diffusion-bonded heat exchangers such as Printed Circuit Heat Exchanger (PCHEs) or Hybrid Heat Exchangers (H^2X) as the heat source heat exchanger (sodium-to-CO_2) as well as the recuperator and cooler modules. Although PCHEs and H^2Xs have a high degree of structural integrity, the potential for leaks to develop between the sodium and CO_2 coolant channels in the heat exchanger cannot be ruled out, and this would lead to discharge of high pressure CO_2 into the secondary coolant circuit. Due to the robustness of the PCHE design, catastrophic failure leading to CO_2 jet blowdown into the secondary sodium loop is not deemed likely. Rather, small cracks (or micro-leaks) may develop in which CO_2 will bleed into the secondary system at a relatively low rate and chemically react with the sodium.

The goal of the sodium-CO_2 interaction tests is to gain a fundamental understanding of sodium-CO_2 interactions under prototypical conditions of compact diffusion-bonded heat exchanger failure, a fundamental understanding of self-plugging if it occurs, and the development of one-dimensional phenomenological models for the interactions between high-pressure CO_2 issuing into liquid sodium from a micro-leak across a stainless steel pressure boundary. These models will be validated using experiment data.

Therefore, an experiment program at Argonne was initiated in Fiscal Year 2010 to investigate the reaction behavior between sodium and CO_2 under micro-leak conditions. Several reports have described the facility scaling rationale and design. Assembly of the SNAKE (S-CO_2, Na Kinetics Experiment) began in Fiscal Year 2011 and was completed in July 2012. The sodium inventory in this facility consists of approximately 44 lbs (20 kg; ~21 L/5.5 gal).

The first sodium-CO_2 interaction experiment was carried out at SNAKE in September 2012. This test was successful in that supercritical carbon dioxide was sparged into a pool of sodium through a 64 µm diameter nozzle.

A series of sodium-CO_2 interaction experiments were carried out in Fiscal Year 2013 in the SNAKE experiment. These tests successfully injected supercritical carbon dioxide into a pool of sodium through a 64 µm diameter nozzle. A reaction between the CO_2 and sodium was detected. The extent of this reaction was unexpected since the initial sodium temperature was 145 ˚C, a temperature range where previous researchers have detected little or no chemical reaction between these species. The important difference between the SNAKE experiment and previous research is that the SNAKE geometry and conditions promote high-interfacial area and mixing between the CO_2 and sodium. These features are likely important in promoting accelerated chemical reactions and will be studied further as the SNAKE test matrix is carried out.

After the FY 2013 experiments, attempts to drain the test vessel into the dump tank were unsuccessful. Mechanical cleaning of the drain line to encourage drainage of test vessel was also unsuccessful due to the presence of large amounts of solid reaction products in this line. During inspection of the test vessel, a mixture of sodium and sodium/CO_2 reaction products were found to fill the vessel up to approximately 76 cm (30 inches) above the injection nozzle. Chemical analysis revealed that the reaction products were primarily composed of

sodium carbonate and sodium oxide. The reaction products appeared to take on a matrix or solid-foam geometry with pure sodium contained within the foam's pores. Phase change could not be used to clean the test vessel since the melting points of the carbonate and oxides, are well above the maximum operating temperature of the vessel. Thus, mechanical or chemical means are the only options for cleaning the test vessel. Since the original test vessel and dump tank configuration had a complex geometry that made such cleaning challenging, simplified vessels were designed and procured in FY 2014.

The revised SNAKE apparatus design philosophy was simplicity and interchangeability. The new test vessel and dump tank are extremely simple and minimize penetrations and other places for sodium and reaction products to become trapped with the goal of making cleaning relatively straightforward. The new SNAKE design substantially reduces the number of fittings, components, and superfluous vessel penetrations. Vessel heating and insulation can be assembled and disassembled quickly which will facilitate rapid changeout of vessels.

A single, well characterized sodium-S-CO_2 interaction experiment was carried out in FY 2014. Supercritical CO_2 was injected into sodium for 1334 s (22.2 min). This experiment was the first to approximate conditions prototypical of a SFR coupled with an S-CO_2 Brayton energy conversion cycle. The initial S-CO_2 injection pressure and temperature were 16.0 MPa and 296 ˚C, respectively. The initial sodium temperature and height were 332 ˚C, and 51.5 cm, respectively. The S-CO_2 was injected through a 75.0 µm nozzle. The total CO_2 mass injected was approximately 121.6 g.

No CO_2 was detected during the course of the experiment above the detection threshold, which strongly suggests that nearly all of the injected CO_2 reacted with sodium. A peak CO concentration of 2.6% was observed which further corroborates substantial sodium and S-CO_2 reaction.

Temperature measurements indicated a bulk sodium temperature increase of approximately 30 ˚C due to the exothermic reaction heat produced. For the first time in a sodium experiment, fiber optic distributed temperature sensors (DTS) were used to successfully measure sodium temperature with unprecedented spatial resolution. Also for the first time, these sensors were shown to clearly indicate the interface between sodium and the gas space which makes them a promising sensor for level indication.

No plugging of the micro-nozzle was detected during this experiment. Data from these experiments are reported and initial analyses of the data are discussed in this report. Additional analysis of this data and improvements of the data quality and facility control will take place in early Fiscal Year 2015.

An updated experiment matrix was developed and is presented. Several experiments are planned for FY 2015. Additionally, model development and validation are planned to begin in Fiscal Year 2015.

Table of Contents

EXECUTIVE SUMMARY ii
List of Figures v
List of Tables viii
1 Introduction 9
2 Fiscal Year 2014 Improvements to SNAKE 10
2.1 Simpler apparatus design 11
2.2 All New Test Vessel and Dump Tank 12
2.3 Improved nozzle geometry 15
2.4 New temperature measurement technique 18
3 FY 2014 Fundamental sodium S-CO_2 interaction experiments 21
4 Chemical analysis of reaction products from FY 2013 experiments 37
5 Non-reactive gas-into-liquid jets – water rig experiments 41
6 Updated near-term detailed test matrix and near-term improvements 46
6.1 Near-term improvements and other non-experiment work 47
7 Summary 48
Acknowledgements 49
References 50

LIST OF FIGURES

Figure 1: Recent photograph of the SNAKE experiment at Argonne. 11

Figure 2: Original (left) and new (right) SNAKE apparatus designs. The new SNAKE design substantially reduces the number of fittings, components, and superfluous vessel penetrations. The new test vessel is simply a pipe fitted to a vessel head on top and a blind hub with several connections on the bottom. 12

Figure 3: Original (left) and new (right) SNAKE test vessel designs. The new SNAKE test vessel is simply a pipe fitted to a vessel head on top and a blind hub with several connections on the bottom. 13

Figure 4: New two-piece band heaters for heating the test vessel. Each band heater is rated to 1200 W, has a wire braid construction, and has one Type K thermocouple in each half to control and monitor heater temperature. 14

Figure 5: Original (left) and new (right) SNAKE dump tank designs. The new SNAKE dump tank is a vertical 8-inch diameter pipe with an ANSI flange on top to facilitate easy access and cleaning. 15

Figure 6: Original (left) and new (right) SNAKE CO_2 injection nozzle designs. The new SNAKE nozzle 16

Figure 7: Drawing of nozzle design that will facilitate S-CO_2 injection into a small channel of sodium. The sodium channel will be representative of a H^2X compact diffusion-bonded heat exchanger geometry and make it possible to evaluate whether the sodium-CO_2 reaction has the potential to plug a HX channel. This nozzle geometry will be tested in FY 2015. 16

Figure 8: Updated P&ID for the new SNAKE setup 17

Figure 9: Drawing showing nozzle, thermocouple rake, and fiber optic distributed temperature sensor (DTS) as installed for the FY 2014 experiment. Dimensions are in cm 19

Figure 10: Schematic of high-temperature DTS in glass capillary 20

Figure 11: New nozzle design concept which will be used in FY 2015 experiments. Two stainless capillaries contain fiber optic distributed temperature sensors for high-resolution temperature measurements in the sodium near the nozzle. 21

Figure 12: Gas flowrates for the FY 2014 sodium S-CO_2 interaction experiment, Exp2014_01 at the S-CO_2 injection nozzle inlet, argon cover gas in, and the exhaust out. 22

Figure 13: Data plots for *"Dry Run #7"* with an empty test vessel (no sodium) and most other parameters similar to the sodium S-CO_2 interaction experiment, Exp2014_01. Time zero is the initiation of CO_2 injection. (a) Gas flowrates for the S-CO_2 injection nozzle inlet, argon cover gas in, and the exhaust out. (b) S-CO_2 and test vessel pressures. (c) Cumulative mass of CO_2 inlet, argon cover gas, and exhaust. (d) Cumulative mass deficit showing all mass accounted for by the conclusion of experiment. (e) Gas mass fractions of CO_2 and CO as measured by the mass spectrometer and thermal acoustic gas analyzer. (f) Thermocouple temperatures near nozzle. 24

Figure 14: Test vessel pressure for the FY 2014 sodium S-CO_2 interaction experiment, Exp2014_01. 25

Figure 15: Temperature history of the sodium column and S-CO_2 nozzle for the FY 2014 sodium S-CO_2 interaction experiment, Exp2014_01. Temperatures of the sodium column were measured by the thermocouple rake and the fiber optic distributed temperature sensor (DTS) at several elevations above the injection nozzle. The S-CO_2 temperature was measured by a thermocouple placed inside the nozzle itself just downstream of the nozzle tip. Uncertainty of the DTS is approximately ±1 ˚C. 25

Figure 16: Contour plot of the DTS data showing temperature at all measured distance above the nozzle vs. time for the FY 2014 sodium S-CO_2 interaction experiment, Exp2014_01. Temperature color scale shown below the plot. Remarkably, the sodium level is extremely well defined in this plot at approximately 52 cm above the nozzle. Sodium level remains essentially constant throughout the experiment. Prior to t=0, the sodium temperature was stratified slightly due to the spacing of the band heaters (the location of one is noted on the left side of this plot). Spatial resolution of the DTS was 2.61 mm and uncertainty was approximately ±1 ˚C 26

Figure 17: Sodium level gamma meter in position with the new SNAKE test vessel setup 28

Figure 18: Sodium level as measured by the gamma level meter in the FY 2014 sodium S-CO_2 interaction experiment, Exp2014_01 29

Figure 19: Cumulative mass flows for the FY 2014 sodium S-CO_2 interaction experiment, Exp2014_01. The S-CO_2 injection nozzle inlet, argon cover gas in, and exhaust outlet are plotted along with the sum of the two inlet mass flows (S-CO_2 plus argon) 29

Figure 20: Cumulative mass deficit of S-CO_2 for the FY 2014 sodium S-CO_2 interaction experiment, Exp2014_01. The mass deficit is calculated by subtracting the cumulative exhaust mass flow from the sum of the cumulative inlet mass flows at any given time 30

Figure 21: Estimates of solids produced throughout the FY 2014 sodium S-CO_2 interaction experiment, Exp2014_01 assuming a stoichiometric reaction 32

Figure 22: Gas fractions of CO_2 and CO at the exhaust line during the FY 2014 sodium S-CO_2 interaction experiment, Exp2014_01. Gas fractions for CO_2 and CO are measured by a mass spectrometer, while a highly sensitive thermal acoustic gas analyzer simultaneously sampled CO concentration up to 1000 ppm 33

Figure 23: Estimated total mass CO produced using mass spectrometer measurements in the FY 2014 sodium S-CO_2 interaction experiment, Exp2014_01. Also shown are theoretical estimates for total CO production using the S-CO_2 mass deficit and stoichiometric reaction approximations 35

Figure 24: Measured vs. predicted S-CO_2 mass flow rates. Predicted flow rates use the standard choked flow method to calculate mass flux at the micro nozzle 36

Figure 25: Pictures of the S-CO_2 injection nozzle (top) before the test and (bottom) after the test showing a significant amount of reaction products and oxides including black particulates 37

Figure 26: Pictures of the S-CO_2 injection nozzle and chunks of products that were removed from the test vessel. One such chunk was sliced in half which revealed a pure sodium core surrounded by a matrix of reaction products and oxides.....38

Figure 27: Schematic depicting titration methodology and species identified during that process.....39

Figure 28: SEM image of a reaction product sample after an ethanol wash. Only sodium, carbon and oxygen were observed which eliminates sources of potential contamination.....40

Figure 29: X-ray Diffraction (XRD) pattern showing observed species and those that were not observed 41

Figure 30: Water test rig setup for visualizing the injection of high pressure gas jets into liquid. (Left) picture of full water test rig and (right) close up near nozzle with gas injection showing gas jet and stainless capillaries for temperature measurement 43

Figure 31: Visualization of CO_2 jets in water (T_{water}=25 ˚C) with the CO_2 pressures being (left) subcritical at 70 bar (T_{CO2}=30 ˚C) and (right) supercritical at 130 bar (TCO_2=41 ˚C) 44

Figure 32: Visualization of S-CO_2 jet in water (T_{water}=25 ˚C) with the S-CO_2 pressure being supercritical at 216 bar (T_{CO2}=34 ˚C).....45

Figure 33: Close up of nozzle and S-CO_2 jet showing cone angle. Water temperature, T_{water}=25 ˚C, and S-CO_2 pressure is supercritical at 130 bar (T_{CO2}=38 ˚C).....46

LIST OF TABLES

Table 1: Key characteristics of the FY 2014 sodium S-CO_2 interaction experiment, Exp2014_01 22
Table 2: Assumed values and properties to test whether the test vessel pressure increase can account for the measured mass deficit 30
Table 3: Certified concentrations of gases used for the FY 2014 sodium S-CO_2 interaction experiment, Exp2014_01 36
Table 4: Results of titrations 39
Table 5: Comparison of thermophysical properties of sodium and water 42
Table 6: Updated detailed near-term S-CO_2/CO sodium interaction test matrix. First seven experiments (in light green) were completed in FY 13 and the 8th experiment, in light blue, is the primary topic of this report 47

1 Introduction

The Department of Energy's Office of Nuclear Energy (DOE-NE) Small Modular Reactor (SMR) program is focused on the development of clean, affordable nuclear power. SMRs have the benefit of lower initial capital investment, scalability, and siting flexibility while also having the potential for enhanced safety and security. The Advanced SMR (aSMR) program contains a spectrum of experimental facilities to support R&D on advanced SMR concepts. One such experiment is the ANL Na-CO_2 Interaction facility, SNAKE (S-CO_2 Na Kinetics Experiment).

The supercritical carbon dioxide (S-CO_2) Brayton cycle, coupled with a Sodium-Cooled Fast Reactor (SFR) SMR, has been identified as a new and innovative energy conversion technology that could contribute to meeting the SMR objectives especially in terms of improved economics. An example is the Advanced Fast Reactor (AFR)-100 SFR SMR design. One appealing feature of this energy conversion system is the smaller footprint that the hardware requires relative to the traditional superheated steam cycle, which is in part due to the small size of the turbomachinery as well as the use of Printed Circuit Heat Exchanger™ (PCHE™) or Hybrid Heat Exchanger (H^2X) compact diffusion-bonded heat exchangers as the heat source heat exchanger (sodium-to-CO_2) as well as the recuperator and cooler modules. Although PCHEs have a high degree of structural integrity, the potential for leaks to develop between the sodium and CO_2 coolant channels in the secondary heat exchanger cannot be ruled out, leading to discharge of high pressure CO_2 into the secondary coolant circuit. Due to the robustness of the PCHE design, catastrophic failure leading to CO_2 jet blowdown into the intermediate sodium loop is not deemed likely. Rather, small cracks (or micro-leaks) may develop in which CO_2 will bleed into the secondary system at a relatively low rate and chemically react with the sodium.

In recognition of the anticipated failure mode for a PCHE sodium-to-CO_2 heat exchanger, an Argonne experiment program, called SNAKE, was initiated in Fiscal Year 2010 (see Farmer et al., 2010; Gerardi et al. 2011, 2012a and 2012b, 2013) to investigate the reaction characteristics between sodium and CO_2 under micro-leak conditions. The goals of the SNAKE facility are to:

1. Determine the fundamental nature and extent of the chemical reactions that occur when high-pressure CO_2 is injected into liquid sodium from a micro-leak across a stainless steel pressure boundary as a function of the sodium pool temperature and inlet CO_2 flowrate,
2. Examine the potential for the micro-leak to seal itself up as a result of blockage formation from the chemical reaction byproducts of the Na-CO_2 reaction, or as a result of oxide layer buildup on the crack faces,
3. Develop one-dimensional phenomenological models for the interactions between high-pressure CO_2 as it issues into liquid sodium from a micro-leak across a stainless

steel pressure boundary. These models will be validated using the experiment data obtained during the completion of the previous two objectives.

An initial test matrix for fundamental sodium (Na)-carbon dioxide (CO_2) interactions was formulated to provide the data needed to understand sodium-CO_2 interactions and their consequences for SFRs incorporating supercritical CO_2 Brayton cycle power converters with compact diffusion-bonded sodium-to-CO_2 heat exchangers (Gerardi et al., 2013). The detailed test matrix recognizes that with the ongoing incorporation of improvements to the facility in Fiscal Year 2013, testing in SNAKE in Fiscal Year 2013 and Fiscal Year 2014 may largely be characterized as shakedown testing, such that testing will need to be extended into following year. This report provides an update on the improvements made to SNAKE in Fiscal Year 2014 and on testing that included sodium-CO_2 interaction experiments where chemical reactions were observed.

2 Fiscal Year 2014 Improvements to SNAKE

A summary of the improvements that were made to SNAKE over the course of Fiscal Year 2014 are included in this section. A recent photo of the entire experiment is shown in Figure 1 where improvements and modifications to the test vessel and dump tank are visible.

In FY 2013, a series of sodium-CO_2 experiments in the first SNAKE test vessel were completed and resulted in significant accumulation of reaction products within the test vessel. The magnitude of these reaction products was a surprise since these experiments were carried out at relatively low temperatures where others (Eoh et al., 2010; Gicquel et al. 2010) had not observed or reported substantial reaction. The primary differences between SNAKE and those previous experiments are that SNAKE injects CO_2 at supercritical pressures and through a small nozzle which creates many small bubbles with corresponding high interface area for chemical reactions.

After the FY 2013 experiments, attempts to drain the test vessel into the dump tank were unsuccessful. Mechanical cleaning of the drain line to encourage drainage of test vessel was also unsuccessful due to the presence of large amounts of solid reaction products in this line. During inspection of the test vessel, a mixture of sodium and sodium/CO_2 reaction products were found to fill the vessel up to approximately 76 cm (30 inches) above the injection nozzle. Chemical analysis revealed that the reaction products were primarily composed of sodium carbonate and sodium oxide. The reaction products appeared to take on a matrix or solid-foam geometry with pure sodium contained within the foam's pores. Phase change could not be used to clean the test vessel since the melting points of the carbonate and oxides, 851 ˚C and 1132 ˚C, respectively, are well above the maximum operating temperature of the vessel, 510 ˚C. Thus, mechanical or chemical means are the only options for cleaning the test vessel. Since the original test vessel and dump tank configuration had a complex geometry

that made such cleaning challenging, simplified vessels were designed and procured in FY 2014.

Figure 1: Recent photograph of the SNAKE experiment at Argonne.

2.1 Simpler apparatus design

The original SNAKE apparatus was designed similar to other sodium experiments with a cleaning loop and dozens of extra ports for addition of instrumentation and adaptability to supplemental experiment objectives. The first set of experiments produced surprisingly large quantities of sodium reaction products and made it clear that the SNAKE experiment was unlike other sodium experiments that maintain high levels of sodium purity. The FY 2013

experiments were completed at relatively low temperatures. Reaction kinetics is expected to increase with temperature, so greater quantities of reaction products are expected in future SNAKE experiments. These reaction products presented a unique design challenge and required a revised test philosophy.

The revised SNAKE apparatus design philosophy was simplicity and interchangeability. The new test vessel and dump tank are extremely simple and minimize penetrations and other places for sodium and reaction products to become trapped with the goal of making cleaning relatively straightforward. The new SNAKE design substantially reduces the number of fittings, components, and superfluous vessel penetrations. Vessel heating and insulation can be assembled and disassembled quickly which will facilitate rapid changeout of vessels. The original and new SNAKE designs are compared in Figure 2. The remainder of this report section describes the new SNAKE design in detail.

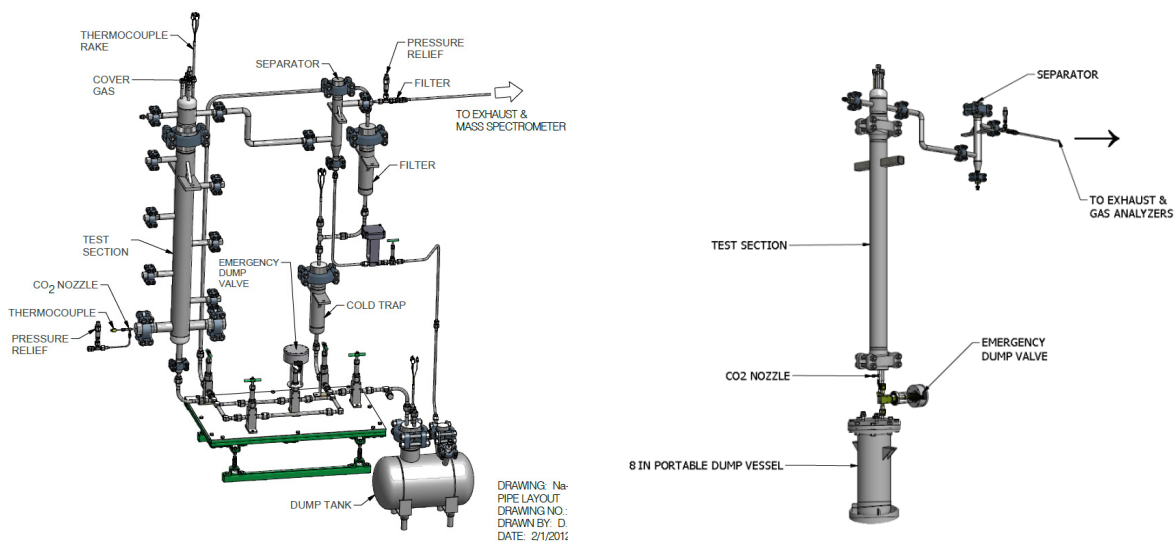

ORIGINAL SNAKE DESIGN NEW SNAKE DESIGN

Figure 2: Original (left) and new (right) SNAKE apparatus designs. The new SNAKE design substantially reduces the number of fittings, components, and superfluous vessel penetrations. The new test vessel is simply a pipe fitted to a vessel head on top and a blind hub with several connections on the bottom.

2.2 All New Test Vessel and Dump Tank

The new test vessel is simply a pipe fitted to the original vessel head on top and a blind hub with several connections on the bottom as shown in Figure 3. Two of these pipe sections were purchased in FY 2014. Additional test vessels may be purchased in FY 2015 so that each experiment takes place in a new, clean test vessel.

The test vessel pipe section has zero penetrations to eliminate regions where sodium and reaction products could accumulate and simplify cleaning. Heating is also simplified with the pipe test vessel design since two piece band heaters (shown in Figure 4) can be used. Each band heater is rated to 1200 W, has a wire braid construction, and has one Type K thermocouple in each half to control and monitor heater temperature. These band heaters can be easily removed and placed on a new test vessel. Thermocouples for data acquisition system (DAS) monitoring are secured to the test vessel using pipe clamps and thermal epoxy. This heating method is significantly faster and less manpower-intensive then the original trace heating method that used magnesia-insulated coaxial heater cable secured to the test vessel using spot welded tabs. The original heating method took approximately one man-month to install while the new heating method takes approximately 10 minutes. Heater equipment costs approximately the same in both cases.

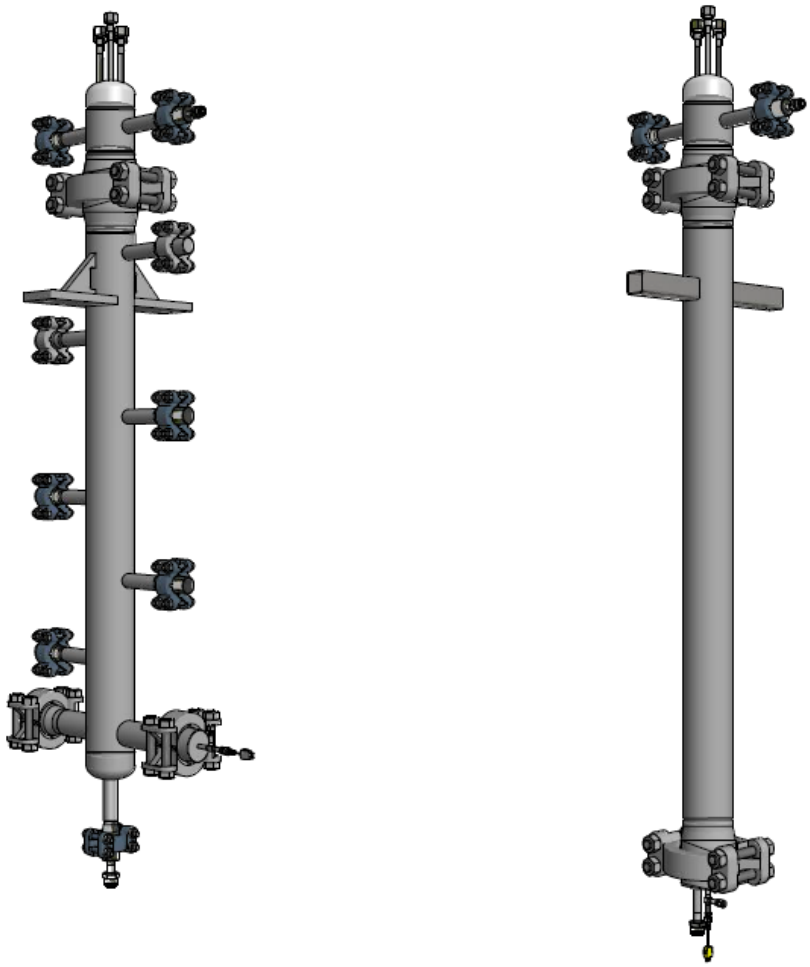

ORIGINAL TEST VESSEL DESIGN NEW TEST VESSEL DESIGN

Figure 3: Original (left) and new (right) SNAKE test vessel designs. The new SNAKE test vessel is simply a pipe fitted to a vessel head on top and a blind hub with several connections on the bottom.

The new test vessels are ASME U stamped according to Section VIII Division 1 of the ASME Boiler and Pressure Vessel Code and carry the same ratings as the original test vessel: 950 ˚F

(510 ˚C) at 450 psig (3.10 MPa). Future vessels may be fabricated in house without an ASME stamp, since Argonne Central Shops is not code certified, in order to reduce the cost of each vessel. They would be fabricated using and complying with ASME code rules with well documented material control, material certifications, and inspections. Since each vessel would be used for approximately a week with a 30 minute test, and would not be operated at the design pressure, this is an affordable path toward accomplishing a number of well-controlled sodium-CO_2 experiments.

Since potential leak paths are most likely through fittings and the number of fittings has been dramatically reduced for the new SNAKE facility, sodium leakage probability has been reduced with the new design.

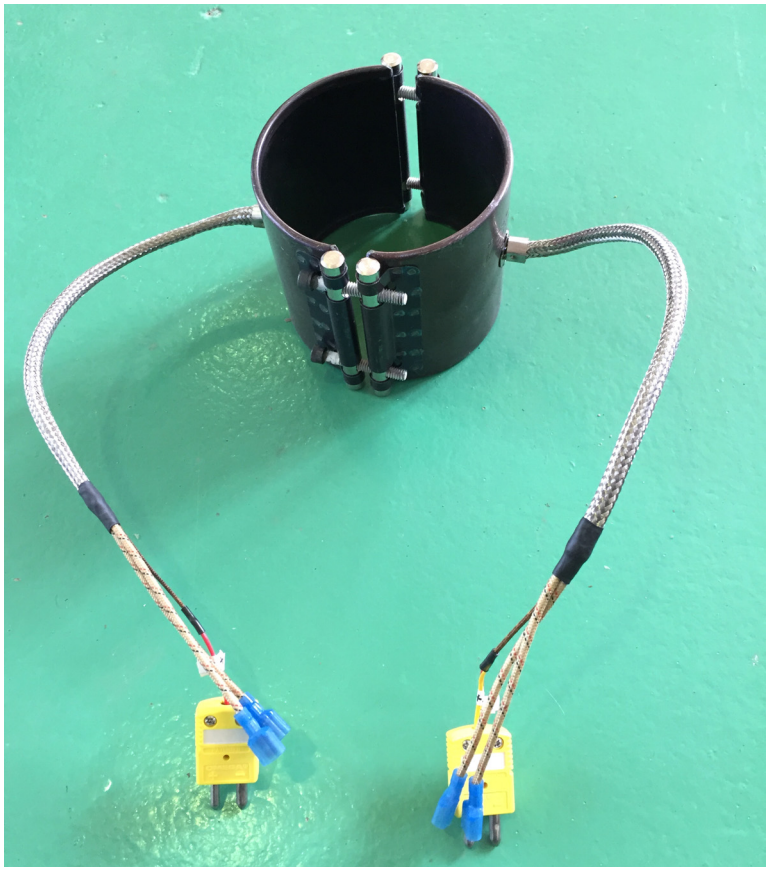

Figure 4: New two-piece band heaters for heating the test vessel. Each band heater is rated to 1200 W, has a wire braid construction, and has one Type K thermocouple in each half to control and monitor heater temperature.

A new dump tank was also fabricated. This dump tank was made to facilitate easy cleaning of sodium and reaction products. A comparison of the original and new dump tank designs is made in Figure 5. Heater installation and flexibility has been vastly improved in a similar way as the test vessel through the addition of band heaters.

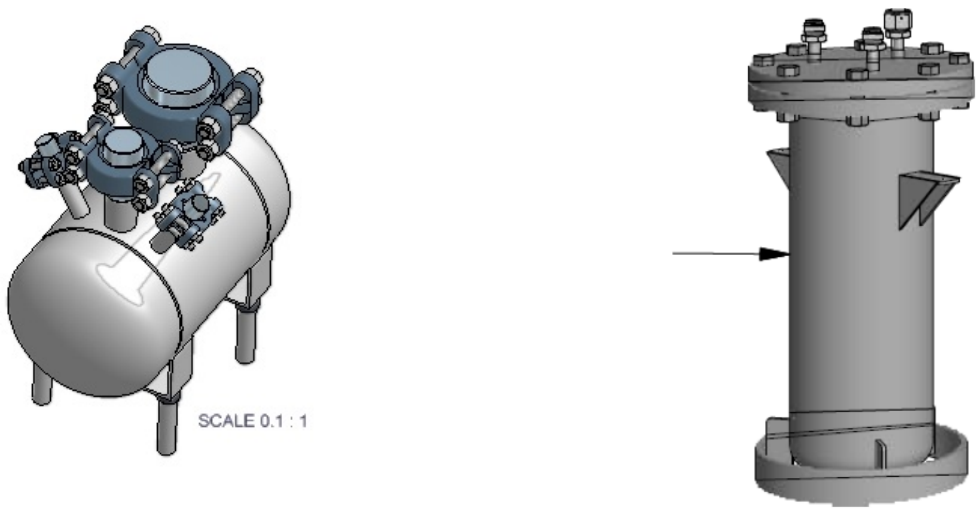

ORIGINAL DUMP TANK DESIGN NEW DUMP TANK DESIGN

Figure 5: Original (left) and new (right) SNAKE dump tank designs. The new SNAKE dump tank is a vertical 8-inch diameter pipe with an ANSI flange on top to facilitate easy access and cleaning.

The new dump tank is a vertical 8-inch diameter pipe and has a large ANSI flange that can easily be removed to enable access to the full inner diameter of the tank. To remove contaminated sodium from this tank, it will be inverted within a sodium passivation hood at Argonne. The flange will be removed, and hand tools will be used to scrape as much material from the tank into a sodium burn tray. If large chunks of material remain, the tank will be heated above the melting point of sodium and the material should flow from the tank into a burn tray. Since this process will be completed in the sodium passivation hood, if a fire should develop, personnel can close the hood door and activate the scrubber unit and safely wait while the fire burns itself out. If most material is successfully removed from the dump tank, it will be removed and carefully cleaned with an ethanol wash. Material in the burn tray will be disposed of per standard passivation procedures.

2.3 Improved nozzle geometry

The nozzle assembly was also improved, redesigned, and fabricated during FY 2014. The original and new SNAKE S-CO_2 nozzle injection assemblies are compared in Figure 6. The new nozzle design makes disassembly straightforward and minimizes the number of welds exposed to liquid sodium.

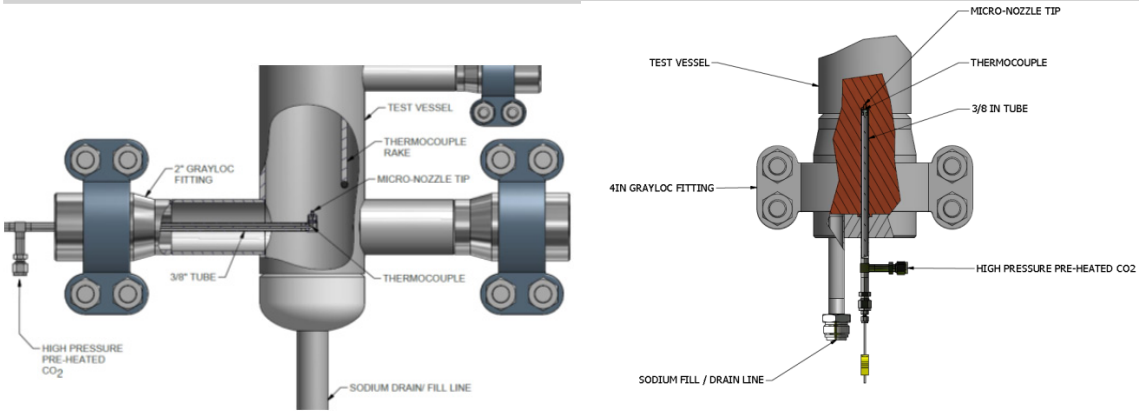

ORIGINAL SNAKE NOZZLE DESIGN NEW SNAKE NOZZLE DESIGN

Figure 6: Original (left) and new (right) SNAKE CO_2 injection nozzle designs. The new SNAKE nozzle .

The new nozzle design is also receptive to tests planned in FY 2015 that involve injection of CO_2 through a microcrack into a small channel of sodium, depicted in Figure 7. The sodium channel will be representative of a H^2X compact diffusion-bonded heat exchanger geometry and make it possible to evaluate whether the sodium-CO_2 reaction has the potential to plug a sodium channel through accumulation of reaction products.

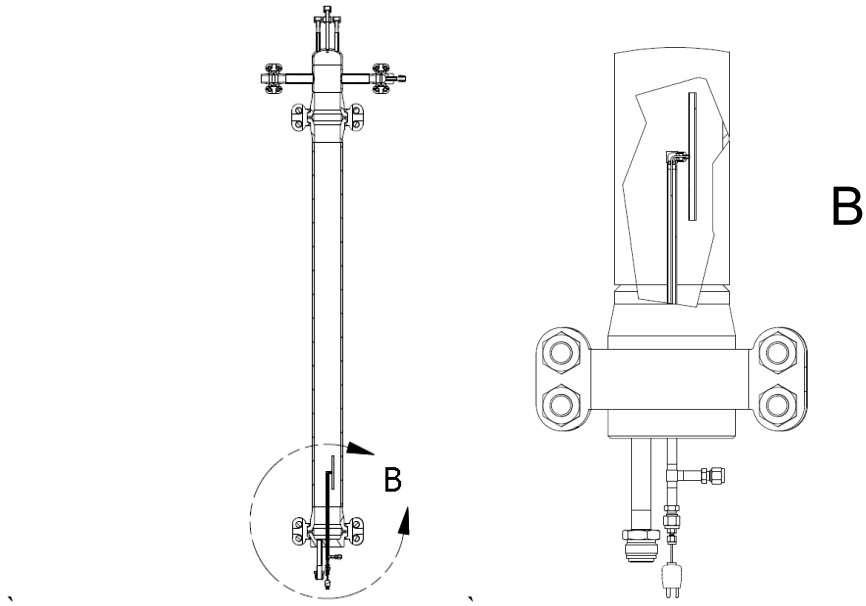

Figure 7: Drawing of nozzle design that will facilitate S-CO_2 injection into a small channel of sodium. The sodium channel will be representative of a H^2X compact diffusion-bonded heat exchanger geometry and make it possible to evaluate whether the sodium-CO_2 reaction has the potential to plug a HX channel. This nozzle geometry will be tested in FY 2015.

The piping and instrumentation diagram (P&ID) for the new SNAKE setup is presented in Figure 8.

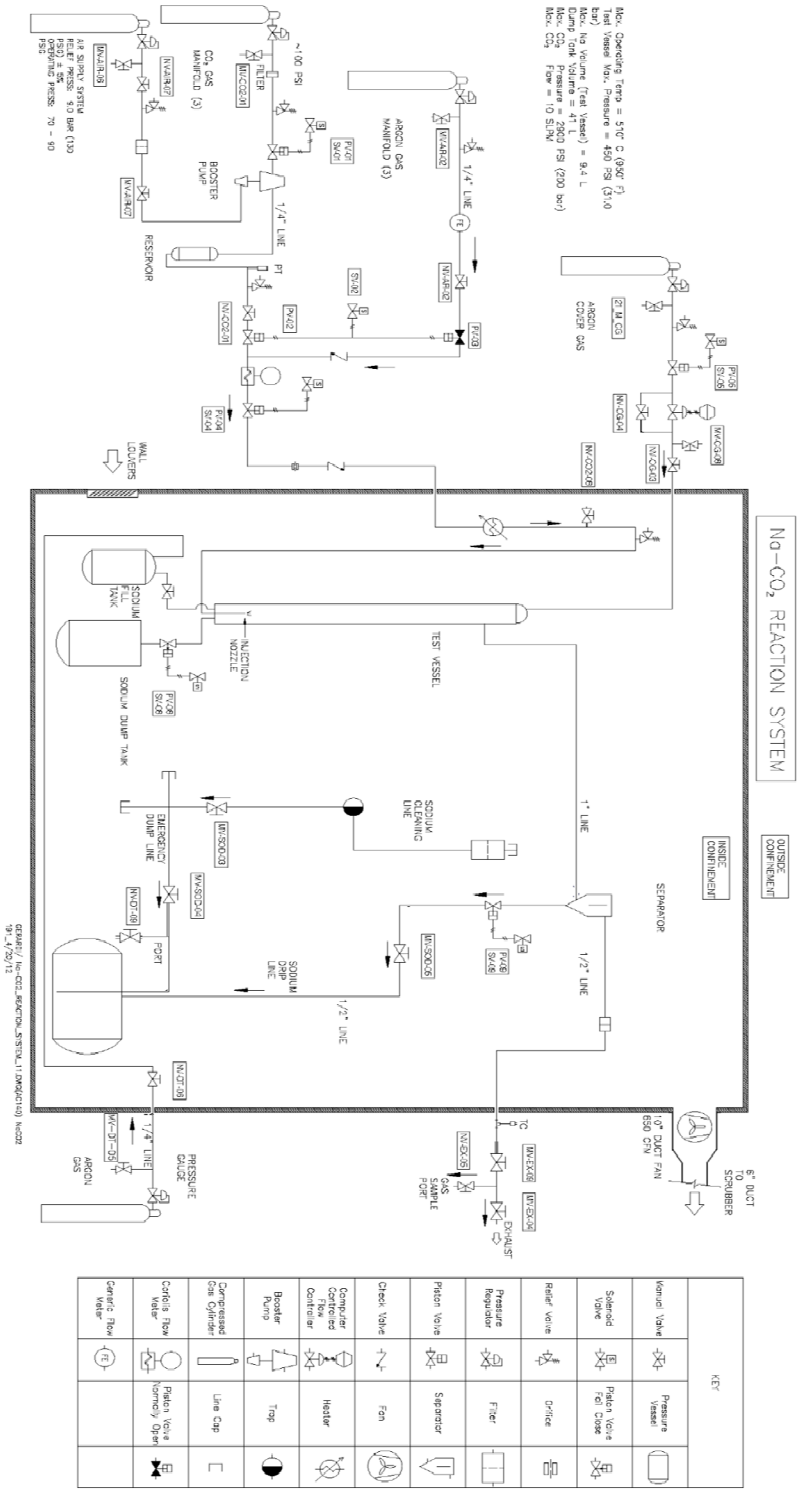

Figure 8: Updated P&ID for the new SNAKE setup

2.4 New temperature measurement technique

One of the objectives of SNAKE is to develop simple dimensional models for the interactions of high-pressure CO_2 as it issues into liquid sodium. In order to characterize the CO_2 jet as best as possible, a relatively new high-resolution temperature measurement technique was added to the SNAKE facility in FY 2014. A relatively new technique for accomplishing this is called distributed temperature sensing based on Rayleigh scattering and swept-wavelength interferometry. Several hundred or thousands of temperature measurements can be acquired along a single strand of thin optical fiber, which is called a distributed temperature sensor (DTS).

A basic description of the DTS technique used in SNAKE is included here while a detailed description can be found in Lomperski et al. (2013), Lomperski and Gerardi (2014), and Lomperski et al. (2014).

Light travelling through a fiber optic waveguide is scattered by impurities and structural variations at the molecular level. The random distribution of these inhomogeneities is stable, giving rise to a backscatter pattern that is unique to the fiber. The spectrum and amplitude of the pattern can be read to serve as a fiber signature and used to interrogate the state of the cable. Physical changes such as strain and temperature shift alter the signature in a repeatable way, and detecting this is the basis for using the fiber as a sensor. This sensing principle has been used to measure temperatures near the core of a research reactor (Sang et al., 2008) and in cryogenic fluids (Boyd et al., 2011).

A tunable laser sends a narrow band signal into the fiber for the purpose of obtaining the resultant backscatter (Gifford et al., 2007). This scattering signal is mixed with a reference signal to generate an interference pattern at the detector. The signal is Fourier transformed to obtain the location of the scattering centers. The amplitude of the backscatter as a function of wavelength is extracted and cross correlated with a baseline signal, or tare. Spectrum shifts are proportional to the strain and temperature according to (Gifford et al., 2007):

$$\frac{\Delta\lambda}{\lambda} = K_T \Delta T + K_\varepsilon \varepsilon \tag{1}$$

where K_T and K_ε are the temperature and strain coefficients, respectively. K_T includes coefficients for thermal expansion and the index of refraction. The thermal expansion coefficient varies with fiber and coating composition and is on the order of 8×10^{-6} K^{-1} for silica fibers.

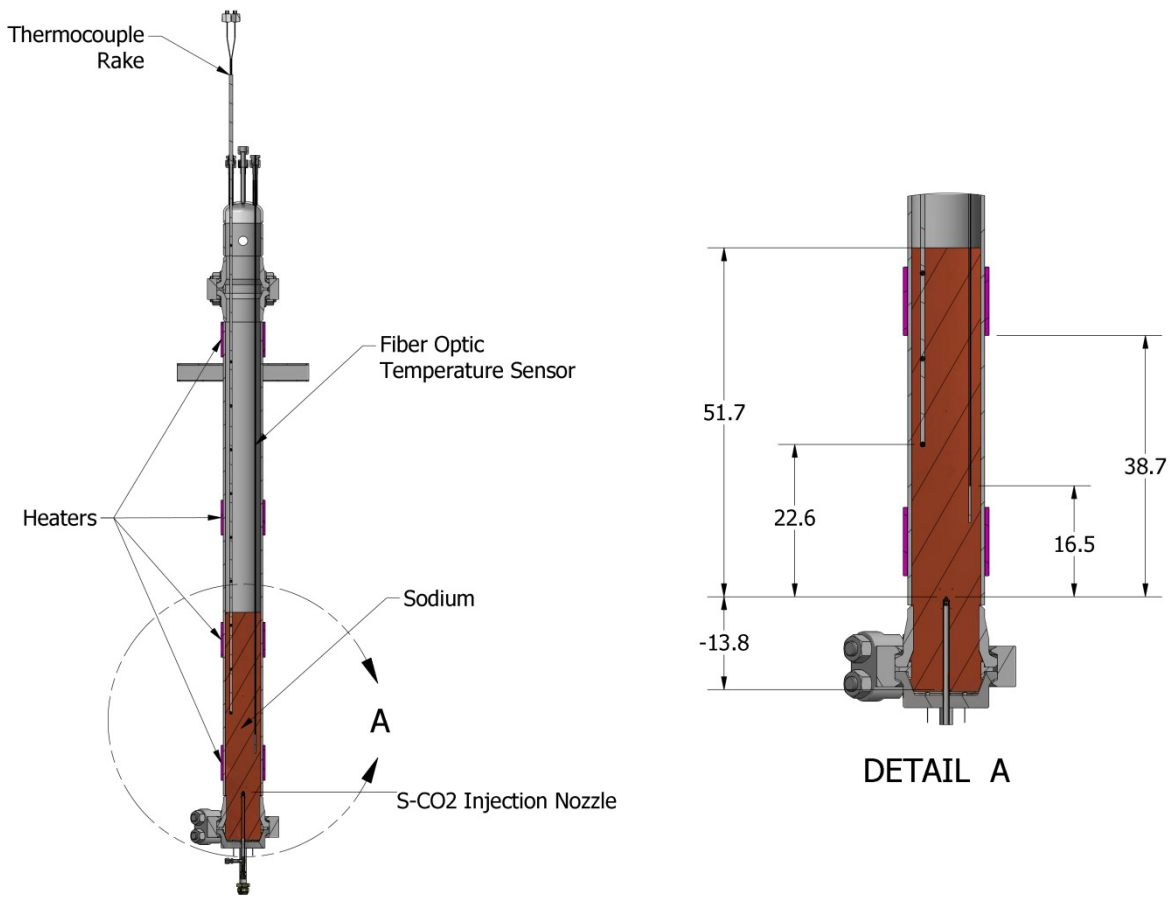

Figure 9: Drawing showing nozzle, thermocouple rake, and fiber optic distributed temperature sensor (DTS) as installed for the FY 2014 experiment. Dimensions are in cm

For the FY 2014 experiment, a single DTS was placed inside a stainless steel capillary parallel to the thermocouple rake as shown in Figure 9. The DTS was manufactured and assembled by Luna Innovations, Inc. (Roanoke, VA). A fiber cable was stripped of all coatings using a sulfuric acid method to obtain a bare glass fiber with 125 µm diameter. A cobalt high-temperature end termination was installed to enable sensing. Without a coating, the bare fiber is extremely fragile so it was immediately installed into a 360 µm OD, 160 µm OD silica capillary and sealed. A schematic of the setup as delivered from Luna is included in Figure 10. At Argonne, the silica capillary with internal fiber was then placed into 1.60 mm OD, 0.056 mm ID stainless tubing. This stainless tube is approximately 1.73 m long and forms the pressure boundary to keep sodium from touching the DTS or leaking to the environment.

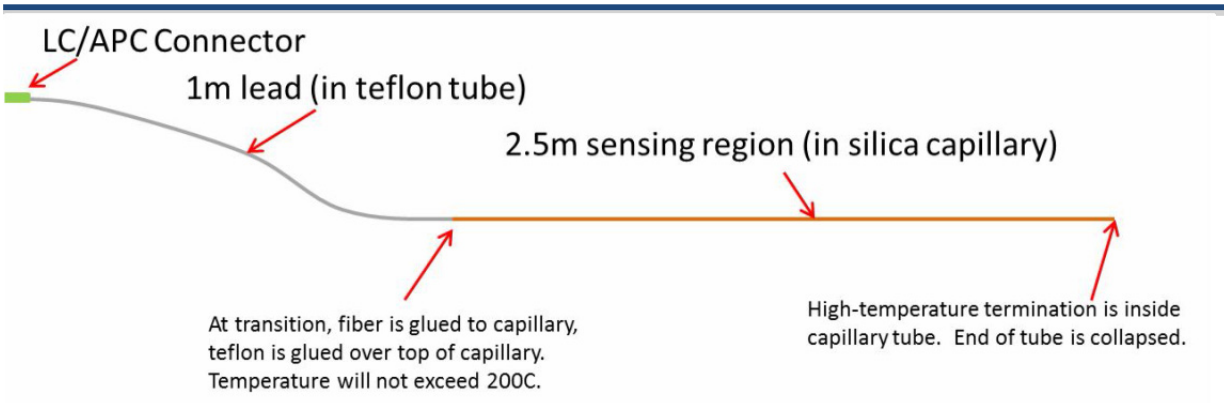

Figure 10: Schematic of high-temperature DTS in glass capillary

A complex DTS setup to measure the sodium/CO_2 temperature very near the nozzle was also manufactured in FY 2014, shown in Figure 11. This nozzle design was actually installed in the FY 2014 experiments but the researchers were unsuccessful in using the capillaries near the nozzle for DTS measurements. The pre-bent capillary shape proved to be a challenge for Argonne's Central Shops to affix to the Grayloc hub to form a pressure boundary. Since the capillaries were small, a brazing process was used. Those brazes handled the sodium environment extremely well; however, the brazing process itself required a cleaning pre-heat step that released the pre-bent capillaries. A second bending step was necessary to re-shape the capillaries after the brazing step which was believed to have created kinks in the capillary ID which made DTS installation extremely challenging. The next nozzle setup, to be used in FY 2015 experiments, will be simplified further and avoid some of the complexities that were challenging the first time around. A larger stainless capillary will be used to make brazing easier and DTS installation painless.

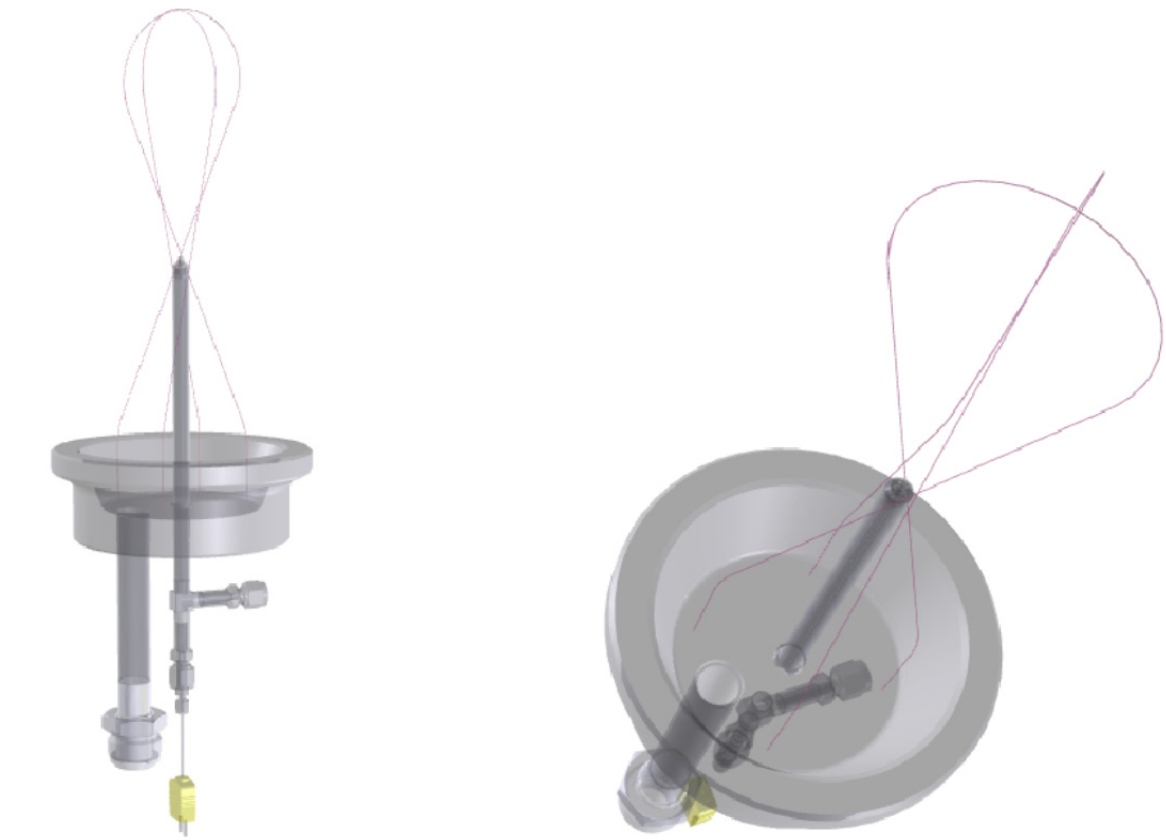

Figure 11: New nozzle design concept which will be used in FY 2015 experiments. Two stainless capillaries contain fiber optic distributed temperature sensors for high-resolution temperature measurements in the sodium near the nozzle.

3 FY 2014 Fundamental sodium S-CO_2 interaction experiments

A single, well characterized sodium S-CO_2 interaction experiment was carried out in FY 2014. Supercritical CO_2 was injected into sodium for 1334 s (22.2 min). This experiment, denoted Exp2014_01, approximated conditions prototypic of a SFR coupled with an S-CO_2 Brayton energy conversion cycle. The initial S-CO_2 injection pressure and temperature were 16.0 MPa and 296 ˚C, respectively. The initial sodium temperature and height were 332 ˚C, and 51.5 cm, respectively. The S-CO_2 was injected through a 75.0 µm nozzle. The total CO_2 mass injected was approximately 121.6 g. Table 1 summarizes these key conditions just before injection, after 1000 s of injection, and just prior to the completion of the experiment at 1334 s. The remainder of this section details measurements and observations made during this experiment.

The initiation of S-CO_2 injection begins at time zero and stops at time 1334 s for all data plotted and analyzed in this Section. Approximately 250 s worth of data prior to S-CO_2 injection is shown in post plots in order to clarify initial conditions.

Table 1: Key characteristics of the FY 2014 sodium S-CO_2 interaction experiment, Exp2014_01

Characteristic	Initial Value at t=0 s	Value at t=1000 s	Value at finish t=1334 s	Units
S-CO_2 pressure	16.0	11.2	10.7	MPa
Sodium temperature	332.0	363.0	355.0	˚C
Sodium height above nozzle	51.5	52.5	52.5	cm
S-CO_2 injection temperature	296.0	310.0	316.8	˚C
S-CO_2 injection flow rate	n/a	289	231	g/hr
S-CO_2 nozzle size		75.0		µm
Cumulative CO_2 mass injected	0	96.3	121.6	g/hr
CO gas fraction	0	0.025	0.022	-

The measured flowrates of the S-CO_2, argon cover gas inlet, and exhaust outlet are shown in Figure 12. Argon cover gas pressure was fixed at 340 kPa and throttled using a needle valve to obtain a constant initial flow rate of 1300 g/hr (12.16 slpm argon).

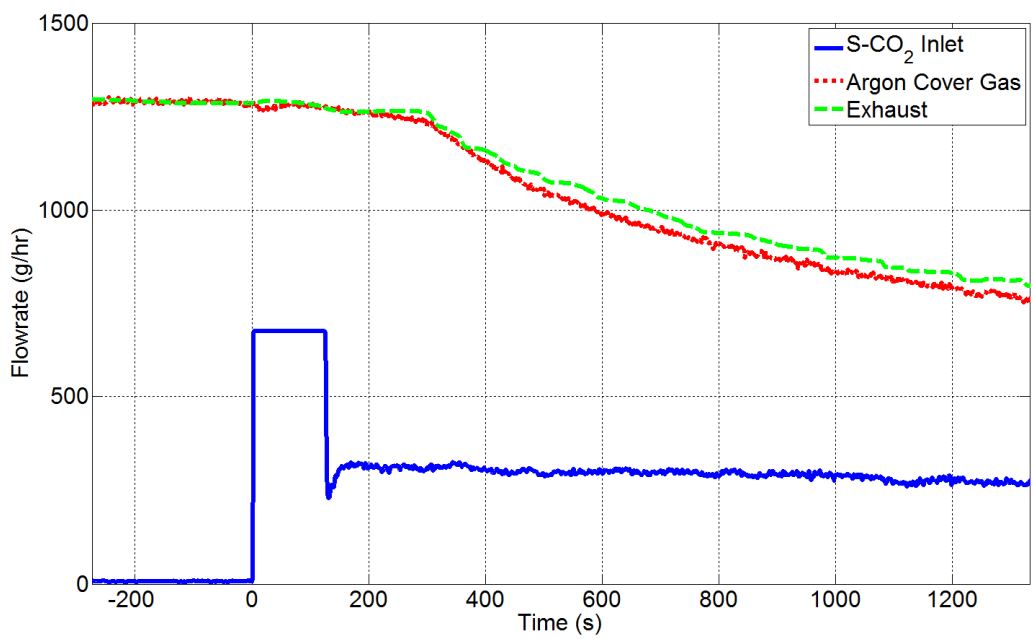

Figure 12: Gas flowrates for the FY 2014 sodium S-CO_2 interaction experiment, Exp2014_01 at the S-CO_2 injection nozzle inlet, argon cover gas in, and the exhaust out.

During dry runs without sodium, the exhaust rate increased as CO_2 injection increased while the argon cover gas flow rate did drop off slightly (see Figure 13(a)) which contradicts the sodium S-CO_2 interaction experiment (Figure 12) where both cover gas and exhaust flow rates dropped after injection began. The only explanation for this drop off was due to a flow restriction on the exhaust line which would increase the pressure drop of the effluent, and also the pressure in the test vessel itself. In fact, a pressure increase in the test vessel was observed, as shown in Figure 14 with a 26 kPa (3.8 psi) increase observed during the course of the experiment, from 296 kPa to 322 kPa. The dry run experiments did not show such an increase (see Figure 13(b)). It is postulated that the sodium S-CO_2 interaction experiment was extremely vigorous and produced a large amount of droplets and aerosols in the form of sodium droplets and entrained solid reaction products. These aerosols likely accumulated in a pipe, separator, or filter. These systems are being inspected carefully to identify the point of holdup and will be cleaned or replaced, accordingly. Future experiments will require careful reconfiguration to avoid this pressure increase since mass balance measurement was challenging. The total mass in the test vessel effectively increases with pressure approximately according to the ideal gas law. This is explored further in a later section.

Temperatures of the sodium column and S-CO_2 nozzle are shown in Figure 15 as observed by the thermocouple rake and DTS setup shown in Figure 9. Both the thermocouple rake and DTS are radially offset from the centralized nozzle by 3.5 cm (1.37) inches as shown in Figure 9. The spatial resolution of the DTS was 2.61 mm and uncertainty was approximately ±1 ˚C. The S-CO_2 temperature was measured by a thermocouple placed inside the nozzle itself just downstream of the nozzle tip. The agreement between the DTS and thermocouple measurements was quite good. Both showed a sharp temperature increase shortly after injection. The sodium column temperature rose approximately 31.0 ˚C in the first 1000 s rising from 332.0 ˚C to 363.0 ˚C at a location 22.6 cm above the nozzle. After the first 1000 s, the temperature gradually dropped to end at 355 ˚C by 1334 s. At the nozzle, the temperature rose from 296 ˚C to 316 ˚C in the first 300 s, dropped back down to 308 ˚C by 500 s and then gradually increased throughout the remainder of the test to 317 ˚C. In the gas space, the temperatures rose approximately 8 ˚C throughout the test. There was some stratification in gas space temperature due to the band heater locations being staggered and regularly cycled since the test vessel was left uninsulated for this test.

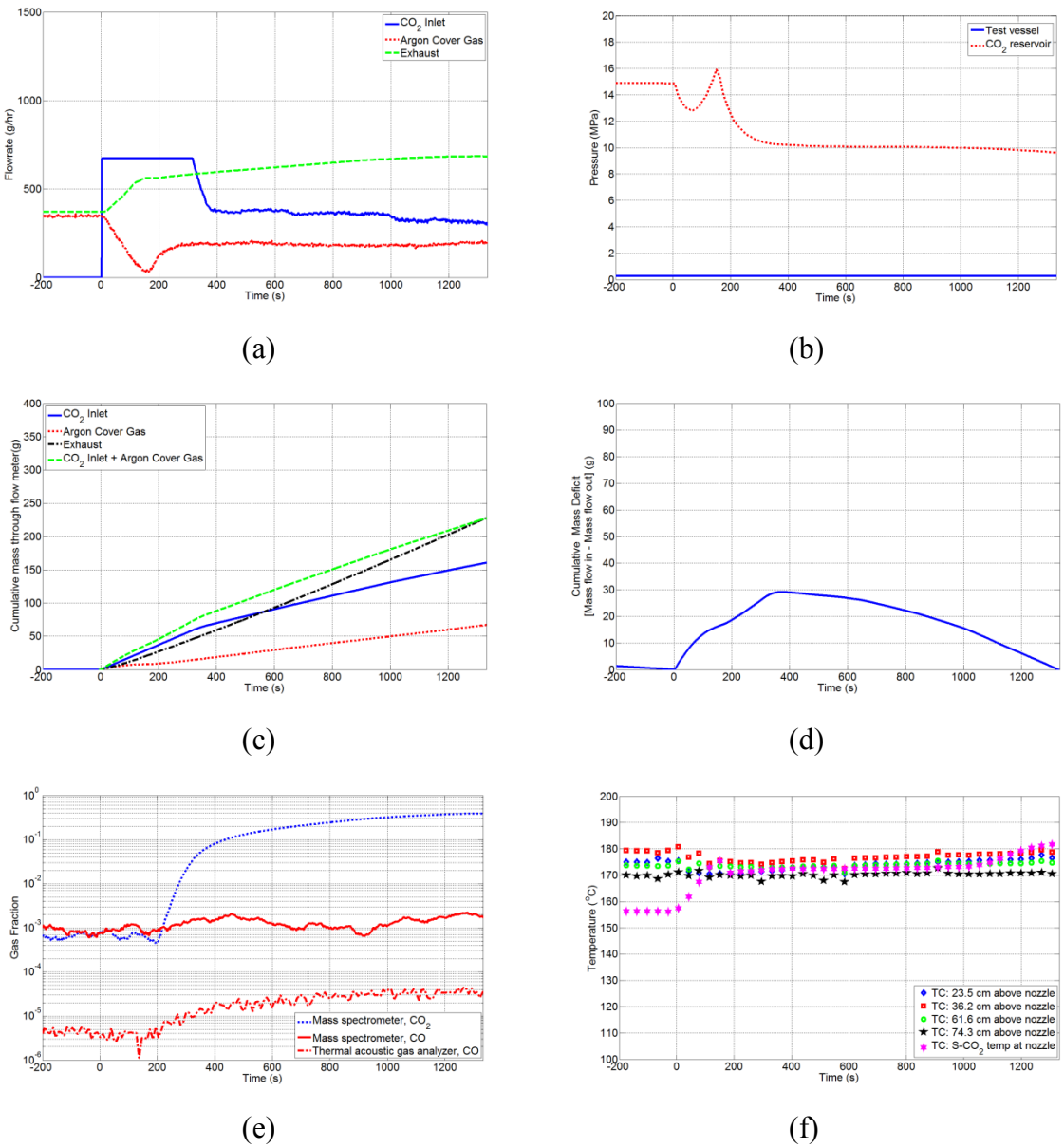

Figure 13: Data plots for *"Dry Run #7"* with an empty test vessel (no sodium) and most other parameters similar to the sodium S-CO_2 interaction experiment, Exp2014_01. Time zero is the initiation of CO_2 injection. (a) Gas flowrates for the S-CO_2 injection nozzle inlet, argon cover gas in, and the exhaust out. (b) S-CO_2 and test vessel pressures. (c) Cumulative mass of CO_2 inlet, argon cover gas, and exhaust. (d) Cumulative mass deficit showing all mass accounted for by the conclusion of experiment. (e) Gas mass fractions of CO_2 and CO as measured by the mass spectrometer and thermal acoustic gas analyzer. (f) Thermocouple temperatures near nozzle.

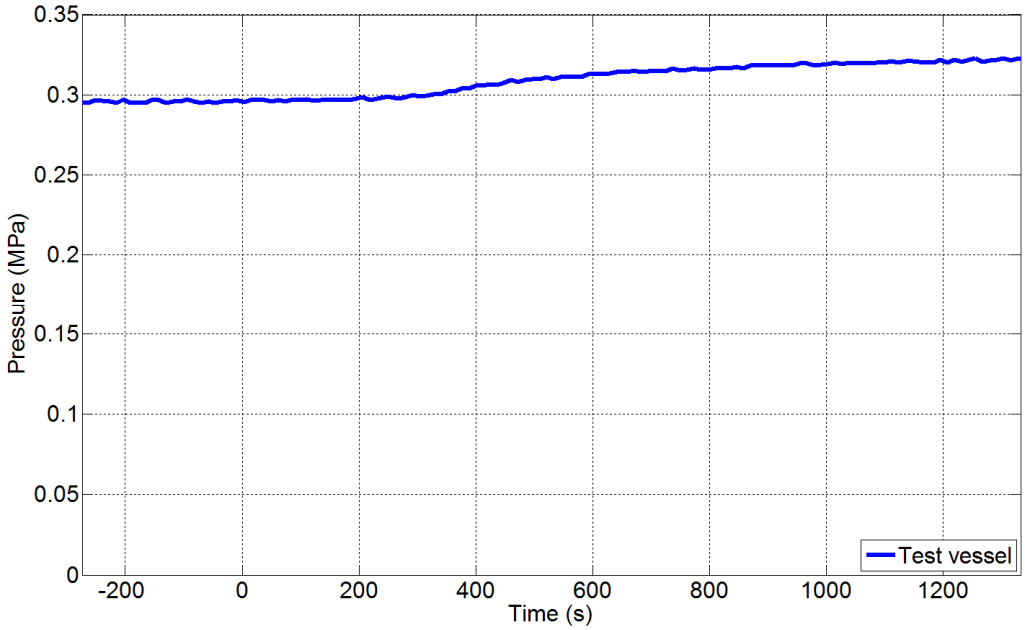

Figure 14: Test vessel pressure for the FY 2014 sodium S-CO_2 interaction experiment, Exp2014_01.

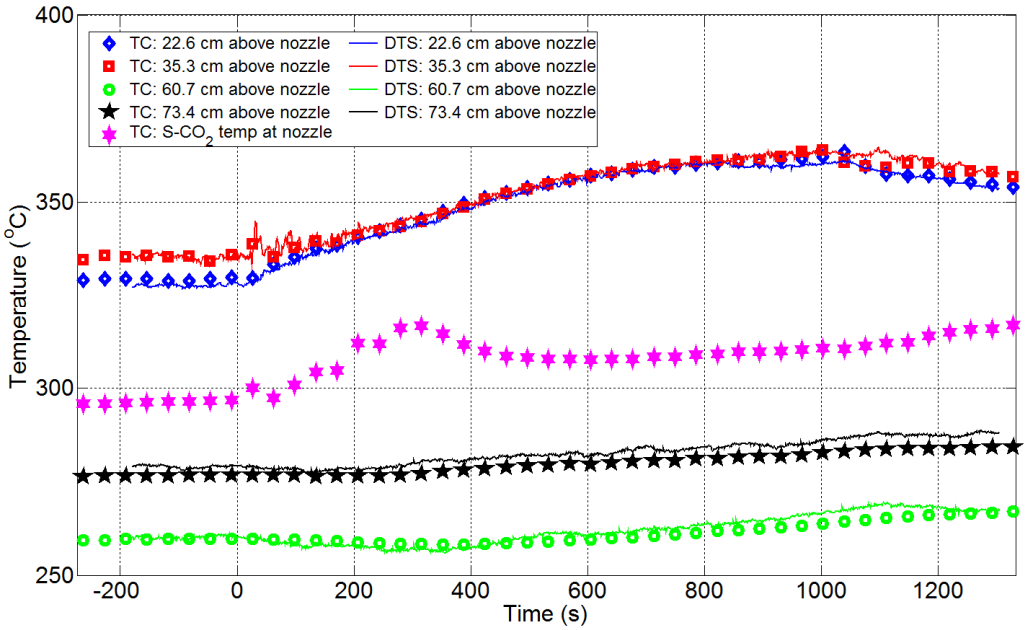

Figure 15: Temperature history of the sodium column and S-CO_2 nozzle for the FY 2014 sodium S-CO_2 interaction experiment, Exp2014_01. Temperatures of the sodium column were measured by the thermocouple rake and the fiber optic distributed temperature sensor (DTS) at several elevations above the injection nozzle. The S-CO_2 temperature was measured by a thermocouple placed inside the nozzle itself just downstream of the nozzle tip. Uncertainty of the DTS is approximately ±1 °C.

To demonstrate the power of the DTS for temperature measurements in a sodium experiment, the DTS data is presented as a contour plot in Figure 16. The x-axis is time while the y-axis is distance above the nozzle since the DTS data is 1-D. The colors denote temperature as shown in the color bar beneath the plot. Remarkably, the interface between the heated sodium and the comparatively cooler cover gas, or the sodium level, is extremely well defined in this plot by the sharp temperature drop approximately 52 cm above the nozzle. Sodium level remains essentially constant throughout the experiment. Prior to t=0, the sodium temperature was stratified slightly due to the spacing of the band heaters (the location of one is noted on the left side of this plot). Spatial resolution of the DTS was 2.61 mm and uncertainty was approximately ±1 ˚C. Sodium level uncertainty is approximately 1.0 cm due to noise in the DTS measurements near sharp temperature gradients. This is the first known use of fiber optic distributed temperature sensors for liquid metal temperature and level measurement. This first attempt demonstrates unexpected potential for using the DTS technique for liquid level measurements. Careful calibration would be unnecessary for most applications since all that is needed is a temperature gradient, which is present in most liquid metal experiments. Of course, this technique is not expected to be useful for applications where the cover gas and sodium temperatures are in equilibrium. Temporal response of the DTS tested is on the order of 1 s.

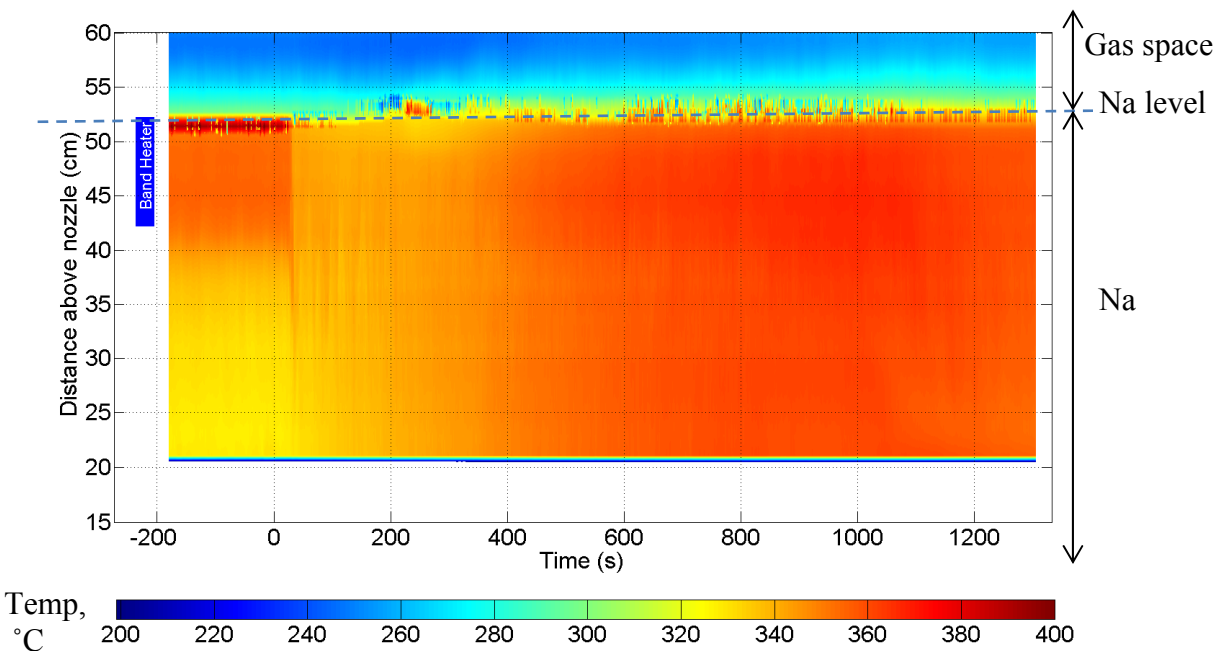

Figure 16: Contour plot of the DTS data showing temperature at all measured distance above the nozzle vs. time for the FY 2014 sodium S-CO_2 interaction experiment, Exp2014_01. Temperature color scale shown below the plot. Remarkably, the sodium level is extremely well defined in this plot at approximately 52 cm above the nozzle. Sodium level remains essentially constant throughout the experiment. Prior to t=0, the sodium temperature was stratified slightly due to the spacing of the band heaters (the location of one is noted on the left side of this plot). Spatial resolution of the DTS was 2.61 mm and uncertainty was approximately ±1 ˚C

The sodium level above the nozzle as measured by the gamma level meter (shown in Figure 17) is shown in Figure 18. Level remains essentially constant throughout the experiment and is consistent with post-experiment physical measurements. The waviness of the sodium level is due to the running average measurement technique used by the gamma level meter. The four cesium sources making up the level meter are extremely small at 0.2 mCi each. Since radioactive decay is a random process, there are occasionally more or less decays at any given time, requiring substantial averaging. In this experiment, the number of counts per second (cps) for the empty and full vessel is 208 and 125, respectively. Thus, only 83 cps separate the full (~1 m) sodium state and empty sodium state. A resolution of 8.3 mm/count is estimated. Practically, the resolution is closer to 5 cm due to random decay. No changes in level were seen during the experiment which is somewhat surprising since particulate generation has been shown to expand sodium volume by five times in previous experiments (Sherman et al., 2002), and the higher density reaction products could influence the gamma level measurement. The DTS measurements do support the gamma level measurement observation of no level change.

Obtaining an instantaneous mass balance using the measured gas flow rates from Figure 12 would have no value since each inlet stream (S-CO_2 and argon cover gas) has a different time lag before reaching the exhaust flowmeter. In a previous publication, Gerardi et al. (2014), used cumulative mass flows for each measurement to identify trends and account for the time it takes for the gases to flow from the inlets to the outlet. This approach is repeated here in Figure 19. These cumulative flows represent the integral flow through each mass flowmeter and start at time zero. A total of 121.6 g of CO_2 was injected, while 371 g of argon was used as a cover gas.

Also shown in this figure is the total inlet mass flow of the S-CO_2 plus the argon cover gas. If no reaction took place, the exhaust mass flow should exactly match the total inlet mass flow by the conclusion of the experiment. In fact, this is observed in the dry run experiment (see Figure 13(c)) where the cumulative inlet flow outpaced the cumulative exhaust flow in the beginning of the experiment but eventually the exhaust caught up. By the conclusion of the dry run experiment, the cumulative mass flow rates were equal. The cumulative mass flow deficit is given by:

$$m_{deficit}(t = n) = \int_0^n \left(\dot{m}_{CO_2,in}(t) + \dot{m}_{Ar,in}(t)\right)dt - \int_0^n \dot{m}_{out}(t)dt \qquad (2)$$

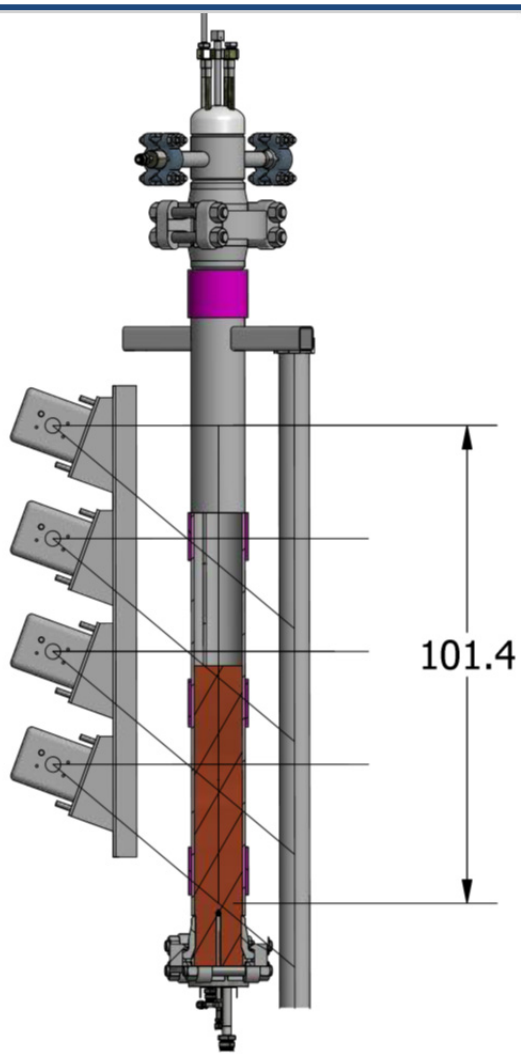

Figure 17: Sodium level gamma meter in position with the new SNAKE test vessel setup

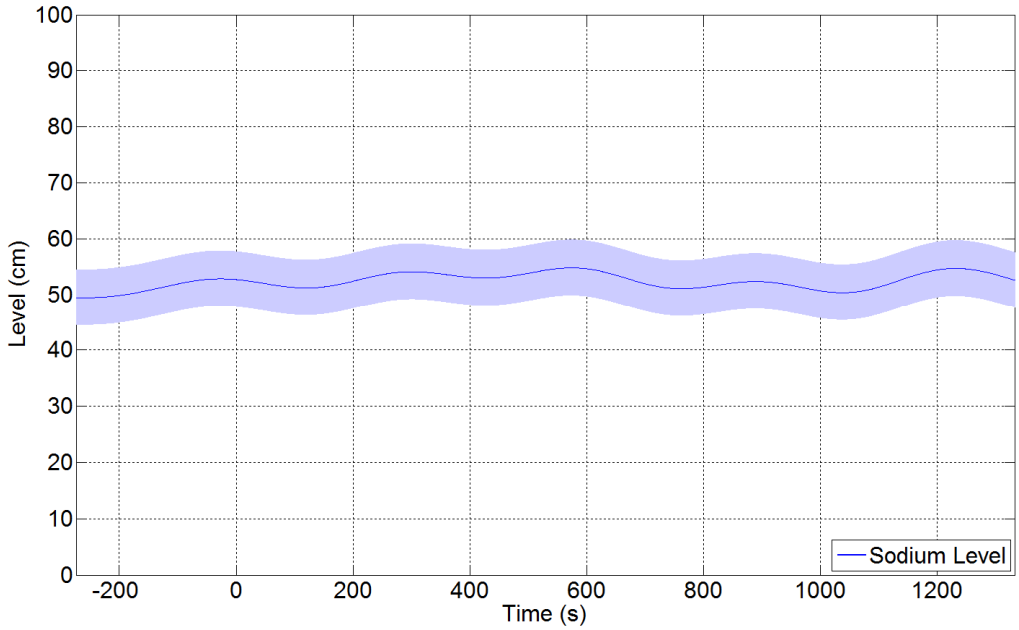

Figure 18: Sodium level as measured by the gamma level meter in the FY 2014 sodium S-CO_2 interaction experiment, Exp2014_01.

In the sodium S-CO_2 interaction experiment, a total mass deficit of 110.5 g is observed over the experiment duration which would correspond to 90% of the injected CO_2.

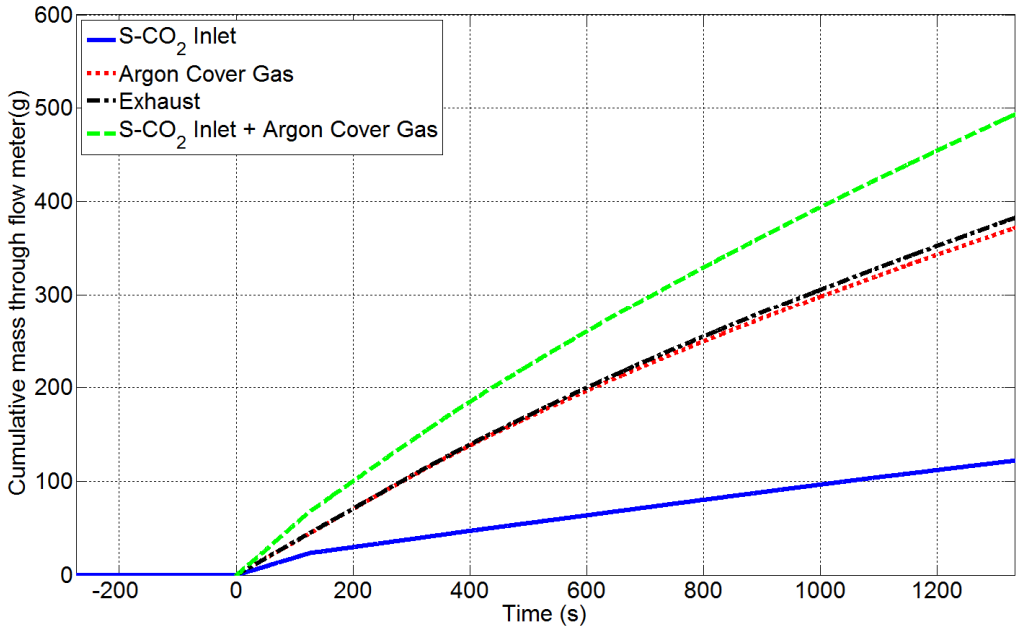

Figure 19: Cumulative mass flows for the FY 2014 sodium S-CO_2 interaction experiment, Exp2014_01. The S-CO_2 injection nozzle inlet, argon cover gas in, and exhaust outlet are plotted along with the sum of the two inlet mass flows (S-CO_2 plus argon)

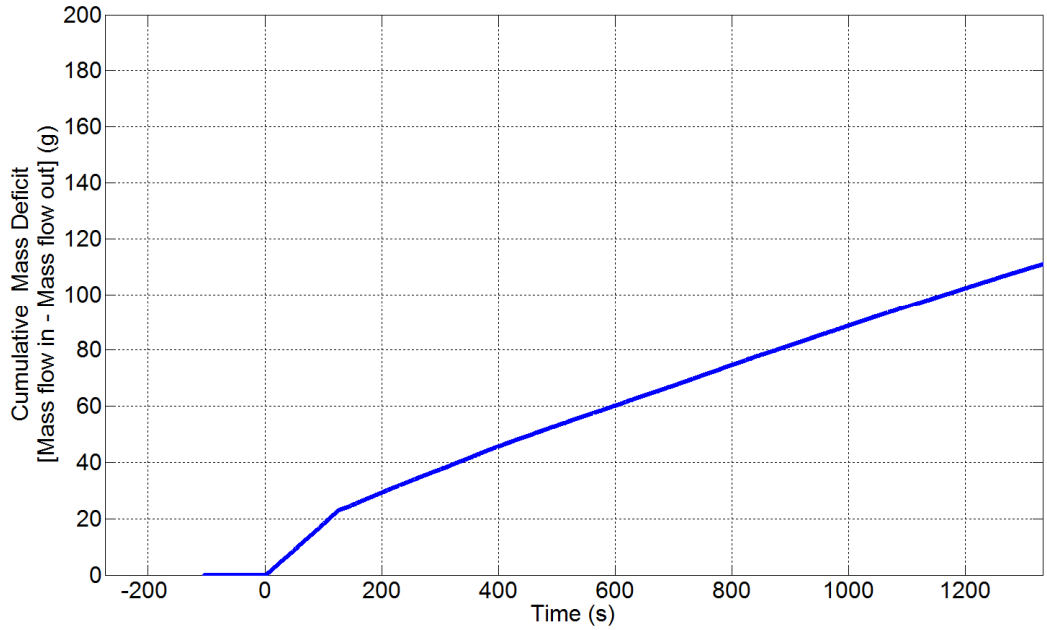

Figure 20: Cumulative mass deficit of S-CO_2 for the FY 2014 sodium S-CO_2 interaction experiment, Exp2014_01. The mass deficit is calculated by subtracting the cumulative exhaust mass flow from the sum of the cumulative inlet mass flows at any given time

As stated above, the test vessel pressure increase could explain this mass increase. To test that theory, the total gas mass increase due to the pressure is estimated. In this case, it is assumed that the test vessel is full of CO_2 only and increases in pressure and temperature according to the measured values in Table 2. The density of CO_2 at the start and finish of the test are also listed in Table 2 according to the thermophysical properties of CO_2 according to the National Institute of Standards and Technology WebBook (NIST, 2013). The density does in fact increase during the test which indicates that some of the injected gas remains in the test vessel and is therefore not measured by the exhaust flow meter. As a conservative estimate, the entire test vessel is assumed to be empty for this calculation, representing 15.4 L. Of course, there is actually sodium in this vessel during the test and there is gas in the exhaust line and separator but the 15.4 L is considered to be a conservative volume for this calculation. The calculated mass is extremely small, on the order of 3.1 g, and does not explain the total mass deficit of 110.5 g that was observed over the course of the experiment. This is one piece of the story that indicates that a significant portion of the injected CO_2 reacted with sodium.

Table 2: Assumed values and properties to test whether the test vessel pressure increase can account for the measured mass deficit

Time (s)	Gas temperature (˚C)	Pressure (MPa)	Density (g/L)	Total gas mass in 15.4 L vessel (g)
0	276	0.296	2.86	44.0
1334	284	0.322	3.06	47.1

Based on the mass deficit of CO_2, it is possible to estimate the total masses of the solids that would be produce should the reaction be stoichiometric. Since the sodium and CO_2 temperatures are well below the high temperature reaction threshold of ~450 ˚C or greater, the following reaction pathway is hypothesized (Gicquel et al., 2010):

$$\begin{aligned} &Na + CO_2 \rightarrow \frac{1}{4} Na_2C_2O_4 + \frac{1}{4} CO + \frac{1}{4} Na_2CO_3 \\ &4Na + Na_2C_2O_4 \rightarrow 3Na_2O + CO + C \end{aligned} \tag{3}$$

Thus, for every mole of CO_2 reacted, one quarter mole of sodium carbonate, Na_2CO_3, will be produced. The oxolate is expected to react immediately with sodium at all temperatures, so for every mole of CO_2 reacted, one quarter mole of elemental carbon and three-quarters of a mole of sodium oxide, Na_2O, will be produced. In order to calculate the masses produced using the above formulations, the molar masses of each molecule must be used appropriately. The formulas used to obtain the quantities of each product are shown below, with m_{XXXX} being the mass of molecule XXXX.

$$m_{Na_2CO_3} = \frac{1}{4} m_{CO_2} \left(\frac{1}{\frac{44g}{mol\, CO_2}} \right) \left(\frac{104g}{mol\, Na_2CO_3} \right) \tag{4}$$

$$m_C = \frac{1}{4} m_{CO_2} \left(\frac{1}{\frac{44g}{mol\, CO_2}} \right) \left(\frac{12g}{mol\, Na_2CO_3} \right) \tag{5}$$

$$m_{Na_2O} = \frac{3}{4} m_{CO_2} \left(\frac{1}{\frac{44g}{mol\, CO_2}} \right) \left(\frac{62g}{mol\, Na_2CO_3} \right) \tag{6}$$

Estimates of the masses of each reaction product produced during the course of the experiment are plotted in Figure 21. Approximately 190 g of total solids were estimated to be produced. The solids product composition includes approximately 117 g of sodium oxide, 65 g of sodium carbonate, and 8 g of elemental carbon.

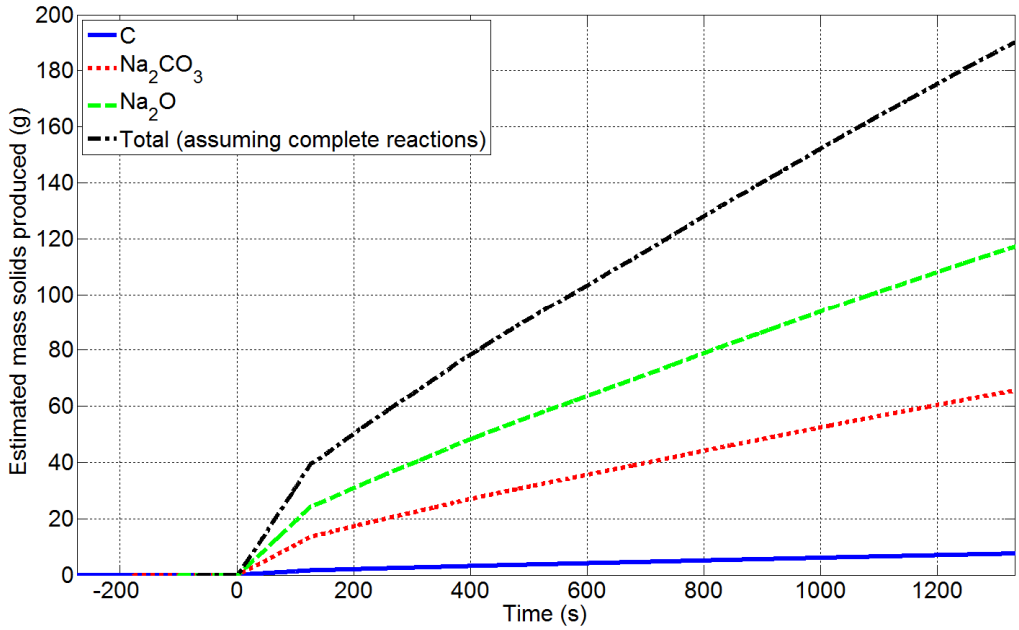

Figure 21: Estimates of solids produced throughout the FY 2014 sodium S-CO_2 interaction experiment, Exp2014_01 assuming a stoichiometric reaction

Note that it is possible that the oxalate did not substantially react during the relatively short duration of these experiments. The reaction between the oxalate and residual sodium could have slowly continued over several hours after the experiment. This is because the sodium was above melting temperature during the ~ 3 hours it took the test vessel temperature to drop below 98 ˚C. Once insulation is placed on the test vessel in future tests, this cool down period will take substantially longer.

All exhaust gas valves were kept closed shortly after the experiment's conclusion to prevent air ingress with a constant argon cover gas pressure maintained. The CO that could be produced by the oxalate reaction with sodium would remain in the test vessel and could further react with sodium as: $2Na + CO \rightarrow Na_2 + C$.

Carbon monoxide was clearly detected during this FY 2014 sodium S-CO_2 interaction experiment, Exp2014_01, as shown in Figure 22. This was an additional indicator that a reaction between the sodium and CO_2 occurred. Carbon monoxide was detected in the 2013 test series (Gerardi et al., 2013) but not during the experiment run in Fiscal Year 2012 (Gerardi et al., 2012.

Two instruments were used to simultaneously measure the concentration of carbon monoxide in the effluent gas. The most sensitive instrument, the thermal-acoustic gas analyzer was installed in Fiscal Year 2013 and detects carbon monoxide from 1 ppm up to 1,000 ppm (gas

fraction of $1x10^{-3}$). After approximately 236 s of CO_2 injection, the gas analyzer CO concentration quickly increases and pegs to its maximum of 1,000 ppm CO for the remainder of the experiment. The minimum sensitivity of the mass spectrometer for CO_2 and CO are 800 ppm (gas fraction of 8 x 10^{-4}) and 1400 ppm (gas fraction of 1.4 x 10^{-3}), respectively. The sensitivity is expected to be further improved in FY 2015. A peak CO concentration of 2.6% (26,710 ppm) is reached at approximately 900 s after injection initiation. No CO_2 is detected during the course of the experiment above the threshold of 800 ppm, which strongly suggests that nearly all of the injected CO_2 reacted with sodium. This result is extremely surprising and contradicts experiments from FY 2014 and also results from other researchers (Gicquel et al., 2010; Gicquel et al., 2010; Eoh et al., 2010) who did not see complete reactions at sodium temperatures below 450 ˚C. During dry runs without sodium, there was a significant amount of CO_2 detected at the exhaust, see Figure 13(e). In fact, the absence of CO_2 detected was so surprising, the mass spectrometer was re-checked after Exp2014_01 to verify it could properly detect CO_2 using a calibration mixture. This check verified that the mass spectrometer remained sensitive to CO_2 concentrations below 1000 ppm, as expected.

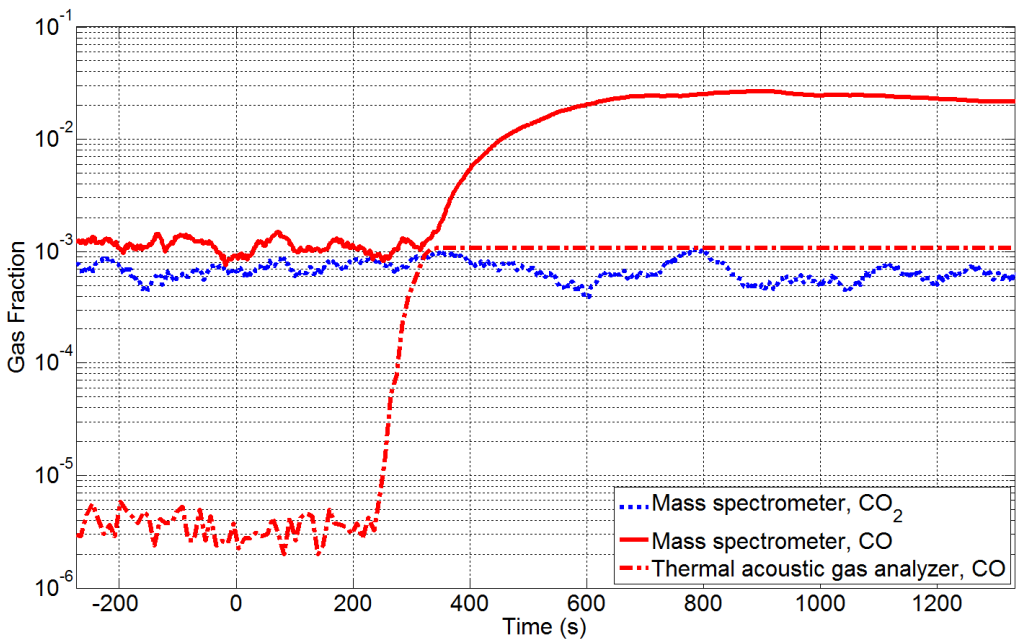

Figure 22: Gas fractions of CO_2 and CO at the exhaust line during the FY 2014 sodium S-CO_2 interaction experiment, Exp2014_01. Gas fractions for CO_2 and CO are measured by a mass spectrometer, while a highly sensitive thermal acoustic gas analyzer simultaneously sampled CO concentration up to 1000 ppm

The carbon monoxide mass flow detected by the mass spectrometer can be compared with the theoretical stochiometric reaction CO production. The CO mass measured can be calculated by multiplying the gas fraction at the mass spectrometer by the exhaust flow rate.

The theoretical CO mass that would be produced if none of the oxalate reacted with sodium can be calculated using Equation 7. In this equation, it is assumed that no oxalate reacts with sodium in order to put a lower bound on the CO production, assuming the CO itself does not react with sodium.

$$m_{CO,nooxylate} = \frac{1}{4} m_{CO_2,defict} \left(\frac{1}{\frac{44g}{mol\ CO_2}} \right) \left(\frac{28g}{mol\ CO} \right) \tag{7}$$

The theoretical CO mass that could be produced if all of the CO_2 that was injected into the system completely reacted can be calculated using Equation 8. In this equation, it is assumed that 100% of the oxylate reacts with sodium in order to put an upper bound on the CO production.

$$m_{CO,oxylate} = \frac{1}{2} m_{CO_2,injected} \left(\frac{1}{\frac{44g}{mol\ CO_2}} \right) \left(\frac{28g}{mol\ CO} \right) \tag{8}$$

The measured and estimated CO production masses are shown in Figure 23. The measured CO production is at least an order of magnitude lower than either of the estimates, which suggests that less CO was produced than predicted by the stochiometry or the CO further reacted with Na to form Na_2O and C.

The gamma level meter was considered and ruled out as a possible source for chemical reactions in Gerardi et al. (2013) since the total activity of the four 0.2 mCi sources is extraordinarily low.

The S-CO_2 injection flowrate, shown in Figure 12, should obey the choked flow assumption since there is a sudden pressure drop across the nozzle from supercritical pressure to nearly atmospheric pressure. To confirm that the measured flow rates are near the theoretical prediction, the predicted flowrates are plotted that use the measured CO_2 inlet temperature and CO_2 pressure to calculate the CO_2 properties at a given pressure. The standard approach for calculating the critical mass flux for a perfect gas from Moody (1990) is used:

$$\frac{P_c}{P_o} = \left(\frac{2}{k+1} \right)^{\frac{k}{k-1}} \tag{9}$$

$$\frac{G_c}{\sqrt{kP_o\rho_o}} = \left(\frac{2}{k+1} \right)^{\frac{k+1}{2(k-1)}} \tag{10}$$

where the gas constant, k, and the density of the fluid, ρ_0, are calculated using the CO_2 properties and the Span and Wagner (1996) equation of state for CO_2. The critical pressure and critical mass flux are represented by P_c and G_c, respectively. The nozzle diameter is 75.0 µm. Thermal expansion in the nozzle is also taken into account by using the thermal expansion coefficient of 316 stainless steel of 16×10^{-6} m/m-K, and a temperature increase from room temperature of 271 K. The total expansion of the nozzle hole is estimated to be 0.352 µm.

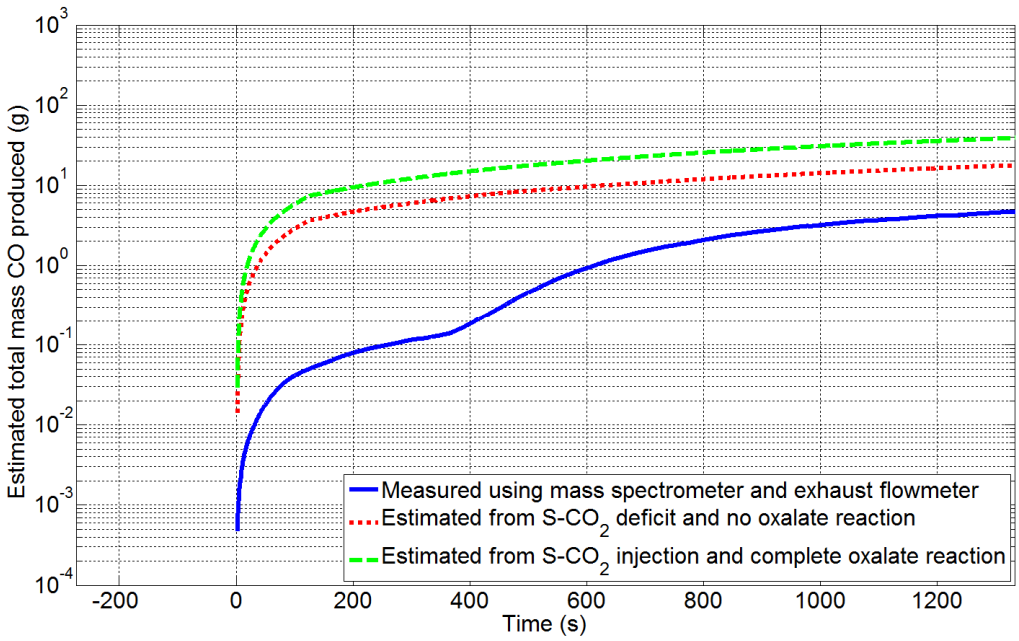

Figure 23: Estimated total mass CO produced using mass spectrometer measurements in the FY 2014 sodium S-CO_2 interaction experiment, Exp2014_01. Also shown are theoretical estimates for total CO production using the S-CO_2 mass deficit and stoichiometric reaction approximations

The predicted mass flow rate using the measured nozzle temperature and measured S-CO_2 pressure at the CO_2 reservoir overpredicts the measured flow rate by well over 30% as shown by the red dotted line in Figure 24. This discrepancy could be due to the crude prediction method, mass flow meter uncertainty, or uncertainty in the other measured parameters. However, the most like source would be in the pressure measurement. The S-CO_2 reservoir is far downstream of the nozzle injection point. The S-CO_2 flows through several restrictions prior to reaching the nozzle including a flow restrictor and the small tubes of the mass flow meter. If a total pressure drop between the measured pressure and the nozzle of 2.1 MPa is assumed, the predicted flow rate follows the measured flow rate very well late in the experiment as shown by the dashed line in Figure 24. This sort of pressure drop is high, but not entirely unexpected especially if a portion of that pressure drop is actually taking place at the nozzle itself since it certainly not an idealized nozzle but has a substantial length of 760 µm (0.030 in), to maintain physical integrity of the pressure boundary. Pressure drops will be

investigated further in FY 2015 to better characterize the actual pressure drop and model the choked flow rate accurately.

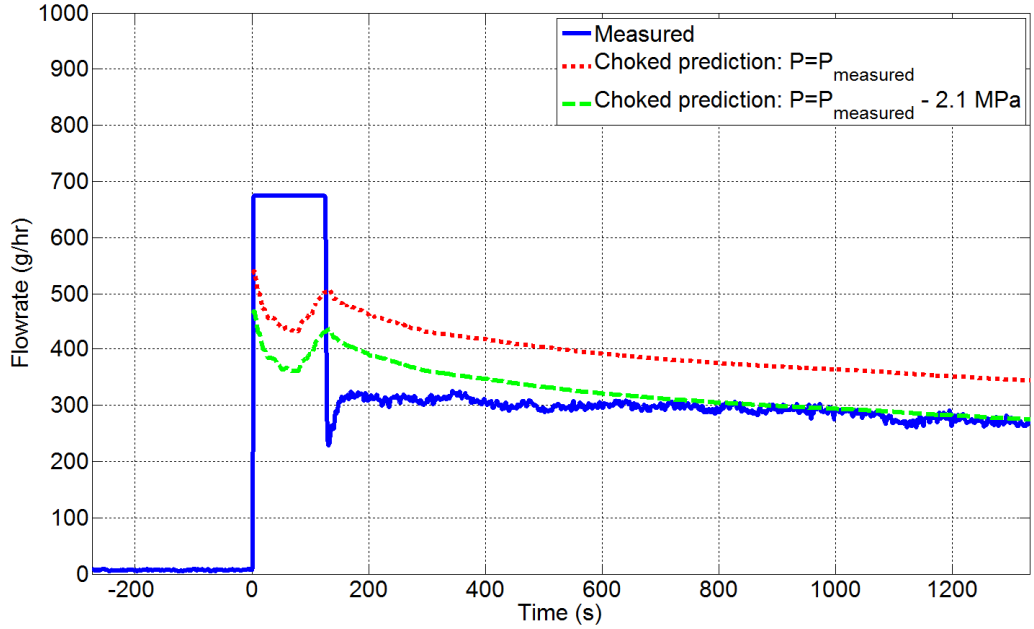

Figure 24: Measured vs. predicted S-CO_2 mass flow rates. Predicted flow rates use the standard choked flow method to calculate mass flux at the micro nozzle

The certified concentrations of the gases used in this experiment are documented in Table 3. Research Grade CO_2 was used for the nozzle injection with purities greater than 99.999%. Built-in-purifier (BIP® Air Products) argon was used for both the cover gas and pre-experiment nozzle injection.

Table 3: Certified concentrations of gases used for the FY 2014 sodium S-CO_2 interaction experiment, Exp2014_01

Gas Injected	Specified Impurity levels				
	Oxygen	Water	Hydrocarbons	Nitrogen	Ar+O_2+CO
CO_2 injected: Research Grade	n/a	< 3 ppm	< 1 ppm	< 5 ppm	< 1 ppm
Ar injected: Built-in-Purifier	< 10 ppb	< 20 ppb	< 100 ppb	< 5 ppm	n/a
	< 10 ppb	< 20 ppb	< 100 ppb	< 5 ppm	n/a

4 Chemical analysis of reaction products from FY 2013 experiments

After the conclusion of the FY 2013 experiment series and cooldown of that test vessel, samples of the sodium and reaction product mixture were obtained and sent to analytical chemistry groups for characterization.

This characterization is ongoing, but some preliminary results are discussed in this section. Pictures of the reaction products are shown in Figure 25 and Figure 26. Sodium, sodium oxide, and a black powder are clearly observed in these pictures. Several large chunks of reaction products were found attached to the nozzle. Several of these chunks were sliced in half which revealed a pure sodium core surrounded by a matrix of reaction products and oxides. After examination of a portion of the test vessel, the researchers believe there is amatrix foam of reaction products and oxides surrounding large pieces of sodium. The reaction product matrix was likely formed during the CO_2 injection at which time sodium was free to flow through the matrix. Once the system was cooled, the sodium froze inside the reaction product pockets which have low strength and can crumble into individual chunks after being mechanically agitated.

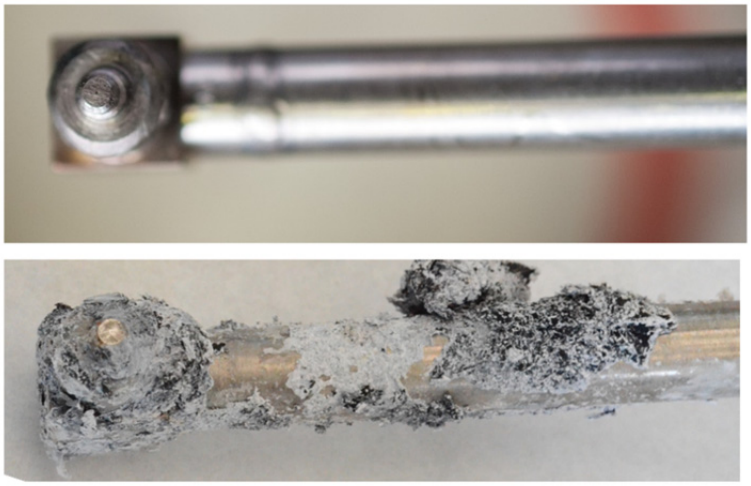

Figure 25: Pictures of the S-CO_2 injection nozzle (top) before the test and (bottom) after the test showing a significant amount of reaction products and oxides including black particulates

Figure 26: Pictures of the S-CO_2 injection nozzle and chunks of products that were removed from the test vessel. One such chunk was sliced in half which revealed a pure sodium core surrounded by a matrix of reaction products and oxides

The titration process is depicted in Figure 27. The sodium samples are first weighed, and washed with ethanol. The solids portion is separated from the liquid portion that includes ethanol and products that reacted and dissolved with ethanol. The liquid ethanol is then run through a standard acid-base titration which allows for quantitative determination of unknown acid or base solutions. The solids portion was then added to water and an acid-base titration was similarly run on that solution. Interestingly, the black substance which clearly survived the ethanol wash completely dissolves or reacts with water. Initially, this substance was believed to be elemental carbon which is a predicted reaction product from the reaction kinetics. However, carbon will not dissolve or react with water in any form. This means the black substance is currently unknown.

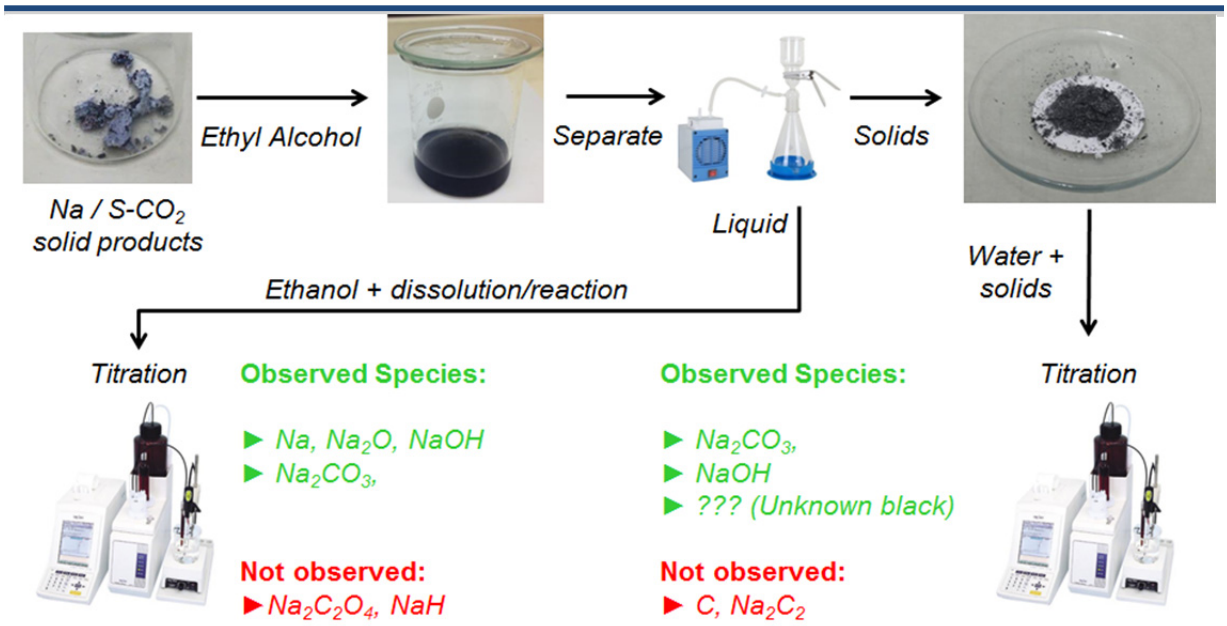

Figure 27: Schematic depicting titration methodology and species identified during that process

The results of the titrations are shown in Table 4 for two samples with initial weights of 100-200 g. Approximately 16-28% of the samples were identified as being Na_2CO_3 and 67-72% as Na. That leaves approximately 5-11% of the samples unaccounted for. Oxalate is not expected to titrate so it could be a portion of the unaccounted mass. However, oxalate is white in color so is not the unidentified black substance.

Table 4: Results of titrations

Sample #	Mass, mg	Na_2CO_3 in Sample, mg	wt% Na_2CO_3 in Sample	Na in sample, mg	wt% Na in sample	Mass unaccounted for, mg	wt% unaccounted
1	192.2	53.4	27.8	129.0	67.1	9.8	5.1%
2	119.9	19.3	16.1	87.0	72.6	13.6	11.3%

One theory for the large amount of reaction products found was that some contaminants entered the system via the gas injection process or due to poor sodium vessel cleaning. Energy-dispersive X-ray spectroscopy (EDS) was used to determine the elemental composition of the products after the majority of the sodium was removed via the ethanol wash. Only sodium, carbon, and oxygen were detected using these processes which are the expected components if no containments were in the system. A scanning electron microscope (SEM) image of the reaction products, taken during the EDS process, is shown in Figure 28.

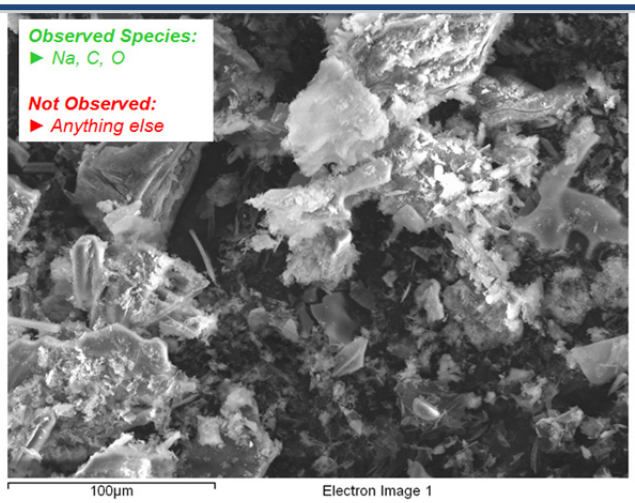

Figure 28: SEM image of a reaction product sample after an ethanol wash. Only sodium, carbon and oxygen were observed which eliminates sources of potential contamination

Lastly, X-ray diffraction (XRD) was used to study the crystalline structure of the reaction products. Products were washed in ethanol in a nitrogen atmosphere and were ground and mounted for XRD analysis. A sample XRD pattern is presented in Figure 29. The species that were possibly observed include Na, Na_2O, NaOH, $Na_2C_2O_4$, Na_2CO_3, $Na_2C_2O_2$, C and Na_2C_2. Products that were not observed include Na_2HCO_3, Na_2CO_4, and $Na_2C_6O_6$. The sample was observed to react with air over the course of the measurement time of one to twelve hours. The reaction was indicated by slow color transition from salt-and-pepper to bright white. A special sample holder was purchased that was designed to be air tight but failed at preventing slow air ingress and resulting reaction. Alternate methods are being explored to keep an inert atmosphere on a new sample while the XRD analysis proceeds.

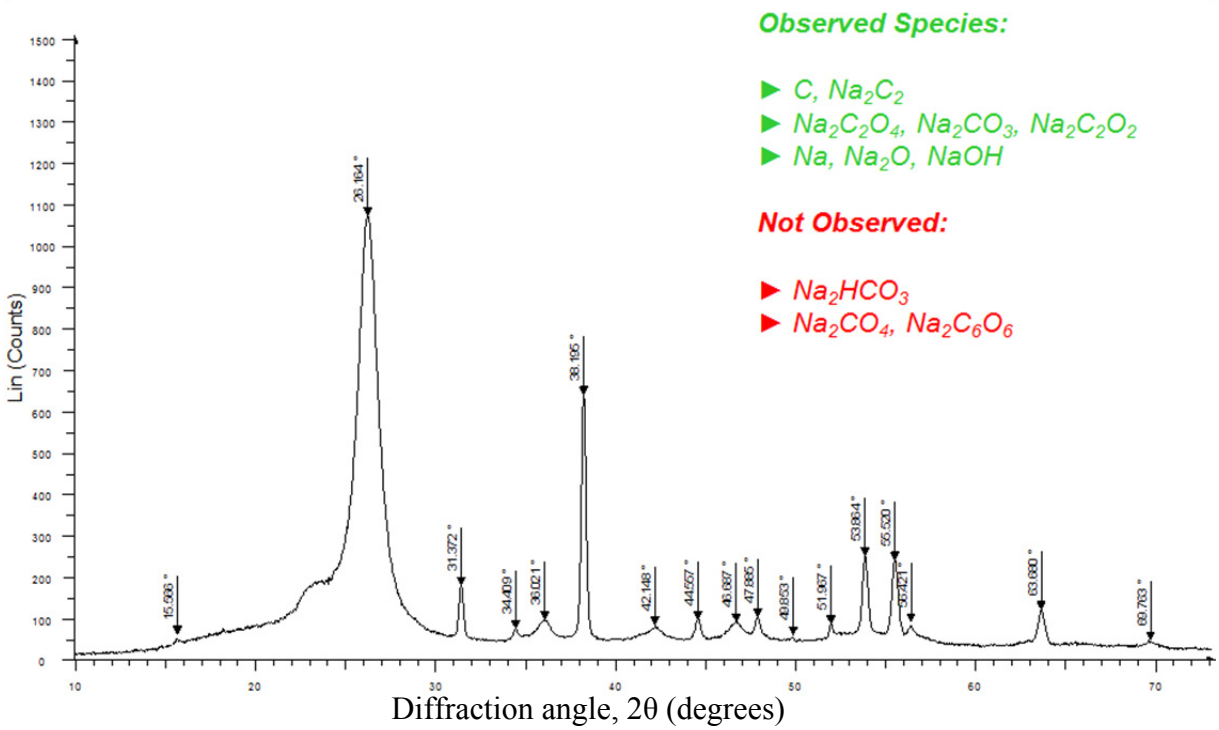

Figure 29: X-ray Diffraction (XRD) pattern showing observed species and those that were not observed

5 Non-reactive gas-into-liquid jets – water rig experiments

Characterization of the two-phase flow regime or pattern is extremely important for modeling purposes. Transitions between flow patterns based upon flow rate alone are ill-defined and subjective since they require visual interpretation.

Choked flow conditions are present in all of the nozzle injection cases considered in the SNAKE experiment matrix since highly pressurized gas is injected into the liquid at approximately atmospheric pressure. The gas speed of sound is reached at the nozzle throat and the gas decelerates as it encounters the liquid pool. For a short distance into the liquid pool, the gas pressure is still considerably higher than the liquid creating an underexpanded zone and local supersonic gas velocities. The slip velocity between the gas and liquid phases in the vicinity of the nozzle is large. The gas-liquid interface is continuously broken up near the nozzle due Rayleigh-Taylor instabilities created by the large phase velocity mismatch. Both the break-off of as bubbles from the gas jet and liquid entrainment within the gas core are expected.

Visualization tests in which S-CO_2 was injected into a cylindrical water pool were completed to attempt to simulate the flow regime of CO_2 injected into sodium. To investigate one of the differences resulting from the property differences between water and sodium, bubble rise

velocities were calculated for water to compare with those for sodium in Figure 3. Relevant thermophysical properties for water (NIST, 2013) at one atmosphere and 25 °C (i.e., room temperature) and 95 °C (i.e., heated water with low subcooling) are compared with those for sodium (Fink and Leibowitz, 1995) in Table 11. At the lower temperature, the water viscosity is significantly greater than that of sodium. The water viscosity is close to that of sodium at the higher water temperature. The water surface tension is significantly lower than that of the liquid metal. However, the water surface tension decreases with increasing temperature such that a higher water surface tension is realized at the lower water temperature.

Table 5: Comparison of thermophysical properties of sodium and water

Fluid	Sodium	Water at 25 °C	Water at 95 °C
Temperature, °C	332	25	95
Density, kg/m^3	873	997	962
Viscosity, Pa·s	3.17×10^{-4}	8.90×10^{-4}	2.97×10^{-4}
Surface Tension, N/m	0.176	0.0720	0.0599

A simple test rig (shown in Figure 30) was constructed to provide visualization of S-CO_2 gas injected into water. The setup is intended to mock-up the SNAKE experiment as closely as possible. The same injection nozzle configuration was manufactured and used in the water rig. The inner diameter of the water tank is the same as the SNAKE test vessel inner diameter, 4 inches (102 mm). Stainless steel capillaries were attached to the nozzle with a similar configuration as the capillaries installed in the bottom blind hub of SNAKE. Distributed temperature sensors were installed in the water rig capillaries and monitored as heated gas was injected into the water. These tests were used to verify that the DTS measurement technique was stable and capable of monitoring temperatures of an underexpanded jet injection into a liquid. No issues were encountered during these temperature measurement tests so the same configuration was applied to the SNAKE system.

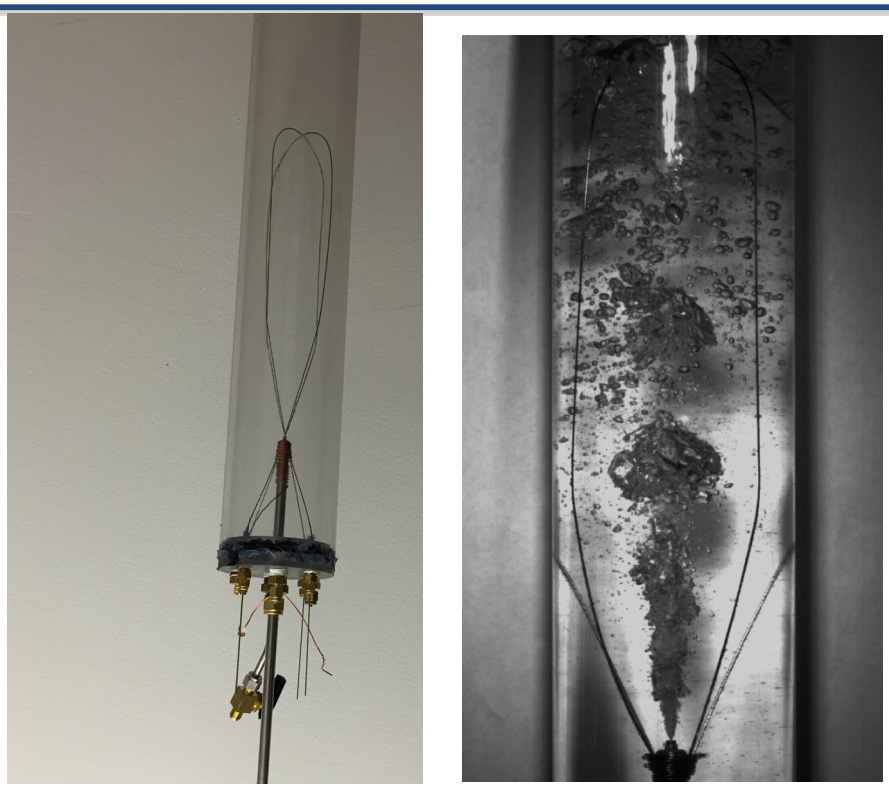

Figure 30: Water test rig setup for visualizing the injection of high pressure gas jets into liquid. (Left) picture of full water test rig and (right) close up near nozzle with gas injection showing gas jet and stainless capillaries for temperature measurement

Several CO_2 injection pressures were visualized from just below the supercritical point up to 200 bar, the expected maximum CO_2 operating pressure in a Brayton energy conversion cycle coupled to an SFR. Two visual observations are shown in Figure 31. The left image shows a CO_2 jet just below the critical point, at 70 bar and 30 ˚C. A gas core is discernable for the first 5 mm from the injector and then further downstream, gas packing decreases and atomization occurs with fine bubbles visible. Some bubble coalescence occurs further downstream prior to the free surface. The right image shows a CO_2 jet well above the critical point, at 130 bar and 41 ˚C. The gas core is discernable for much greater distance, at least 30 mm but possibly all the way to the free surface. The width of the jet is approximately twice as large as in the 70 bar case, approximately 12 mm.

Interestingly, as the pressure was increased from 130 bar to 200 bar, a significant amount of fine gas bubbles were entrained and recirculated which made visualization challenging. A representative image is included in Figure 32, with the S-CO_2 pressure being 216 bar and injection temperature 34 ˚C. The recirculated gas bubbles could actually be more pronounced in sodium since the surface tension of sodium is so high relative to water. This could be one of the reasons a surprisingly large reaction rate in sodium was observed.

The jet cone angle of approximately 20˚ is shown in Figure 33 for a 130 bar S-CO_2 injection pressure. Cone angle did not substantially change for the pressure range of 80 bar to 200 bar.

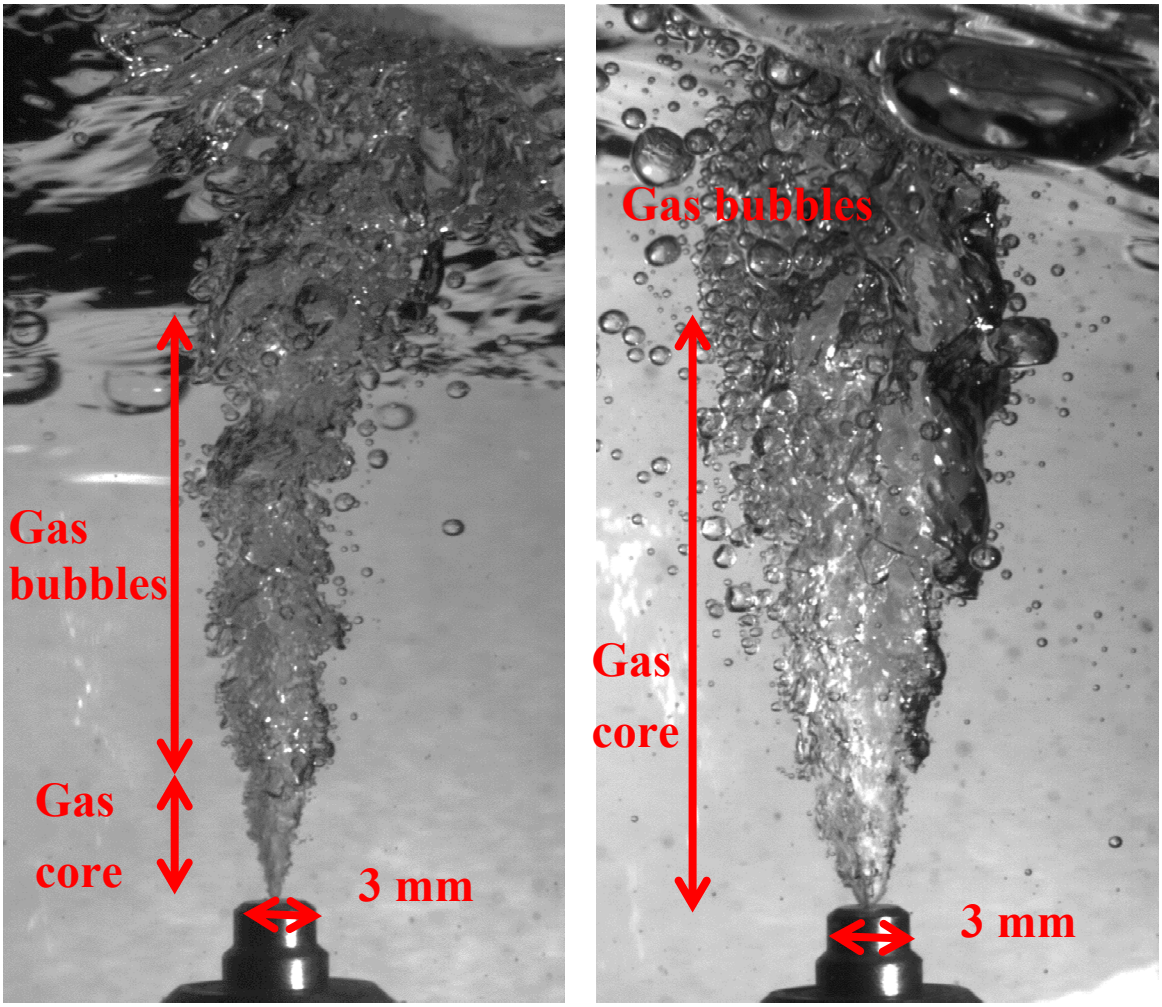

Figure 31: Visualization of CO_2 jets in water (T_{water}=25 ˚C) with the CO_2 pressures being (left) subcritical at 70 bar (T_{CO2}=30 ˚C) and (right) supercritical at 130 bar (TCO_2=41 ˚C)

Figure 32: Visualization of S-CO_2 jet in water (T_{water}=25 ˚C) with the S-CO_2 pressure being supercritical at 216 bar (T_{CO2}=34 ˚C)

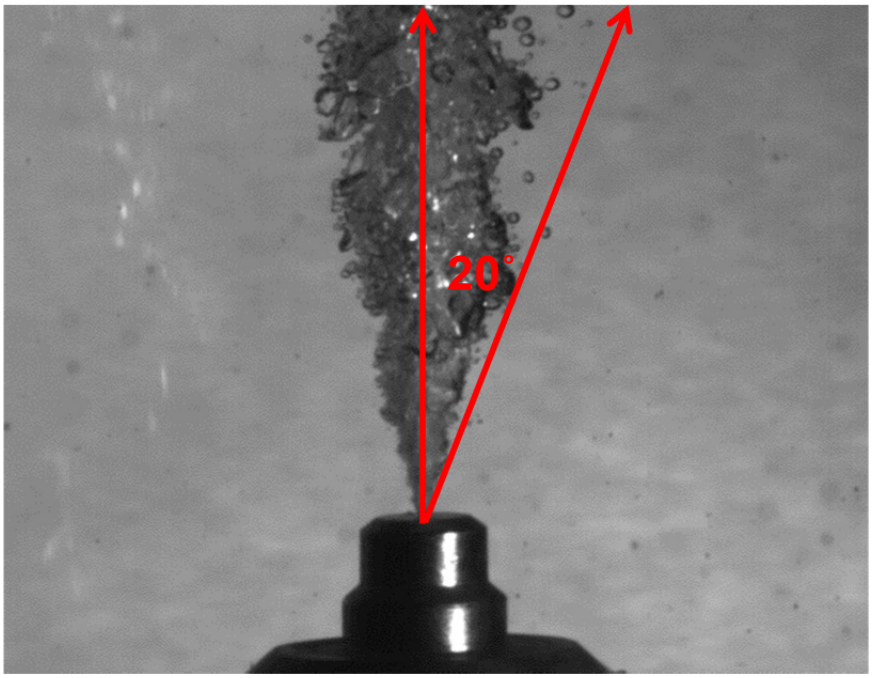

Figure 33: Close up of nozzle and S-CO_2 jet showing cone angle. Water temperature, T_{water}=25 ˚C, and S-CO_2 pressure is supercritical at 130 bar (T_{CO2}=38 ˚C)

6 Updated near-term detailed test matrix and near-term improvements

The general test matrix for SNAKE described in Gerardi et al. (2013) included a near-term test matrix to guide experiments for Fiscal Year 2013 into Fiscal Year 2015. The experiments listed in the near-term test matrix were considered shakedown tests and were designed to obtain useful data; however, data collection was not their primary purpose and would not be considered 'failures' should little useful data arise from the first few tests. The experiments described in the current report were among those shakedown tests, along with those described in Gerardi et al. (2014). The FY 2014 experiments did yield very useful data. These experiments also will be used to update the near-term test matrix to obtain high-quality data for modeling purposes with the smallest number of experiments.

A summary of the completed experiments and the target conditions of the next several experiments are listed in Table 6. All of these tests will be direct injection of CO_2 or CO/CO_2 mixtures into a static sodium pool. Low pressure (sub-critical) CO_2 tests will also be carried out to add to the simulation verification database. Most tests will last approximately 1-30 minutes, or until steady state is reached on all primary instruments.

The first experiment was completed in September 2012 and summarized in Gerardi et al. (2012b). The next six tests were carried out in Fiscal Year 2013 and detailed in Gerardi et al.

(2014). Most of the remaining near-term tests listed in Table 6 do correspond to tests recommended in the general test matrix detailed in Gerardi et al. (2013). It is expected that slight deviations from what is listed in Table 6 will occur as the experimental reality on a given day and the results of previous tests are taken into account.

Table 6: Updated detailed near-term S-CO_2/CO sodium interaction test matrix. First seven experiments (in light green) were completed in FY 13 and the 8th experiment, in light blue, is the primary topic of this report

CO_2/CO injection from micro-nozzle into open sodium pool								
Test #	Test year	Test Gas	Gas initial stagnation pressure, MPa	Gas stagnation temperature, ˚C	Sodium column temperature, ˚C	Sodium column height, cm	Injected gas mass, g	Test duration, min
1	2013	CO2	9	170	180	38.1	247	30
2	2013	CO2	2.8	143	141-145	46.8	7.8	4.2
3	2013	CO2	6.1	146	141-184	48.4	48.5	4.2
4	2013	CO2	7.6	144	142-216	53.6	61.4	4.2
5	2013	CO2	8.6	146	143-242	55.0	87.9	4.2
6	2013	CO2	10.1	145	145-253	54.9	39.1	4.2
7	2013	CO2	11.3	145	145-259	53.7	40.5	4.2
8	2014	CO2	15	300	332	51.5	120	22
9		CO2	15	300	330	20.0	-	20
10		CO2	20	300	330	50.0	-	20
11		CO2	15	450	450	20.0	-	5
12		CO2	15	380	380	20.0		20
13		CO2 w/ H2X Channel Geometry	15	300	330	50.0	-	20
14		CO	15	300	330	20.0	-	5
15		CO	15	300	330	50.0	-	5
16		50% CO/50% CO2	15	300	330	50.0	-	5
17		CO2	11	450	450	20.0	-	5
18		CO2	15	145	145	40.0	-	5
19		Nitrogen	Sodium level detector testing and gas hold-up experiment			10-90	-	-

6.1 Near-term improvements and other non-experiment work

Near-term improvements that are anticipated for Fiscal Year 2015 and other non-experiment work are summarized here in list form. These improvements are expected to continue in parallel to the continued sodium S-CO_2 interaction test matrix. As improvements become available they will be taken advantage of for a given test campaign but should not hold up testing.

- A high mass flow CO_2 flow meter will be added to measure the initial injection of CO_2 as it fills the line, displacing argon, between the S-CO_2 valve and the nozzle itself at the start of a test.
- A dampening method will be investigated to allow the Coriolis flow meter to accurately measure flow while the gas booster is active. The initial phase of the test requires an active gas booster to re-pressurize the CO_2 system. The Coriolis flow meter did not measure flow rate accurately during this phase. In the future, it is also desired to actively pump CO_2 in order to maintain a set injection pressure for an extended period of time.
- A larger sodium reservoir will be installed to enable gradual pressure changes to the S-CO_2 inventory

- An insulation jacket will be added around the test vessel setup to limit heat losses. Insulation was intentionally neglected during this test in order to simplify access to the test vessel.
- Several of the heating and tubing setups were temporary as various approaches to obtain the best quality data were explored during the "dry run" test series. The successful setups will be hardwired into place

7 Summary

A series of sodium-CO_2 interaction experiments were carried out in Fiscal Year 2013 in the SNAKE (S-CO_2 Na Kinetics Experiment) experiment. These tests successfully injected supercritical carbon dioxide into a pool of sodium through a 75 µm diameter nozzle. A vigorous reaction between the CO_2 and sodium was detected. The important difference between the SNAKE experiment and previous research is that the SNAKE geometry and conditions promote high-interfacial area and mixing between the CO_2 and sodium. These features could be very important in promoting accelerated chemical reactions and will be studied further as the SNAKE test matrix is carried out.

After the FY 2013 experiments, attempts to drain the test vessel into the dump tank were unsuccessful. Mechanical cleaning of the drain line to encourage drainage of test vessel was also unsuccessful due to the presence of large amounts of solid reaction products in this line. During inspection of the test vessel, a mixture of sodium and sodium/CO_2 reaction products were found to fill the vessel up to approximately 76 cm (30 inches) above the injection nozzle. Chemical analysis revealed that the reaction products were primarily composed of sodium carbonate and sodium oxide. The reaction products appeared to take on a matrix or solid-foam geometry with pure sodium contained within the foam's pores. Phase change could not be used to clean the test vessel since the melting points of the carbonate and oxides, are well above the maximum operating temperature of the vessel. Thus, mechanical or chemical means are the only options for cleaning the test vessel. Since the original test vessel and dump tank configuration had a complex geometry that made such cleaning challenging, simplified vessels were designed and procured in FY 2014.

The revised SNAKE apparatus design philosophy was simplicity and interchangeability. The new test vessel and dump tank are extremely simple and minimize penetrations and other places for sodium and reaction products to become trapped with the goal of making cleaning relatively straightforward. The new SNAKE design substantially reduces the number of fittings, components, and superfluous vessel penetrations. Vessel heating and insulation can be assembled and disassembled quickly which will facilitate rapid change out of vessels.

A single, well characterized sodium S-CO_2 interaction experiment was carried out in FY 2014. Supercritical CO_2 was injected into sodium for 1334 s (22.2 min). This experiment was the first to approximate conditions prototypic of a SFR coupled with an S-CO_2 Brayton energy conversion cycle. The initial S-CO_2 injection pressure and temperature were 16.0 MPa and 296 ˚C, respectively. The initial sodium temperature and height were 332 ˚C, and 51.5 cm, respectively. The S-CO_2 was injected through a 75.0 µm nozzle. The total CO_2 mass injected was approximately 121.6 g.

No CO_2 was detected during the course of the experiment above the detection threshold, which strongly suggests that nearly all of the injected CO_2 reacted with sodium. A peak CO concentration of 2.6% was observed which further corroborates substantial sodium and S-CO_2 reaction.

Temperature measurements indicated a bulk sodium temperature increase of approximately 30 ˚C due to the exothermic reaction heat produced. For the first time in a sodium experiment, fiber optic distributed temperature sensors (DTSs) were used to successfully measure sodium temperature with unprecedented spatial resolution. Also for the first time, these sensors were shown to clearly indicate the interface between sodium and the gas space which makes them a promising sensor for level indication.

No plugging of the micro-nozzle was detected during this experiment. Data from these experiments was reported and initial analyses of the data were completed and discussed. Additional analysis of this data and improvements of the data quality and facility control will take place in early Fiscal Year 2014.

An updated experiment matrix was developed and presented. Several experiments are planned for FY 2015. Additionally, model development and validation are planned to begin in Fiscal Year 2015.

Acknowledgements

Argonne National Laboratory's work was supported by the U. S. Department of Energy Advanced Small Modular Reactor (aSMR) Program under Prime Contract No. DE-AC02-06CH11357 between the U.S. Department of Energy and UChicago Argonne, LLC. The work presented here was carried out under the Energy Conversion Technology area of the aSMR Program. The authors are grateful to Gary Rochau (SNL), the Technical Area Lead, Bob Hill (ANL/NE), the National Technical Director, as well as Brian Robinson (U.S. DOE), the Headquarters Program Manager for the aSMR Program.

References

1. C.D. Boyd, B.D. Dickerson, B.K. Fitzpatrick, "Monitoring Distributed Temperatures Along Superconducting Degaussing Cables via Rayleigh Backscattering in Optical Fibers." In: Proceedings of the Intelligent Ships Symposium IX (ISSIX) Drexel University, Philadelphia, PA USA, (2011).
2. J.E. Brockmann, F.E. Arellano, and D.A. Lucero, "Validation of Models of Gas holdup in the CORCON Code," NUREG/CR-5433, SAND89-1951, Sandia National Laboratories, December, (1989).
3. J.H. Eoh, H.C. No, Y.H. Yoo, J.Y. Jeong, J.M Kim, S.O. Kim, "Wastage and Self-Plugging by a Potential CO_2 Ingress in a Supercritical CO_2 Power Conversion System of an SFR," J. Nuclear Science and Technology, Vol. 47(11), pp. 1023-1036, (2010).
4. M.T. Farmer, D.J. Kilsdonk, J.J. Sienicki, and C. Grandy, "Design of a Test Facility to Investigate Fundamental Na-CO_2 Interactions in Compact Heat Exchangers," ANL-GENIV-164, (2010).
5. C. Gerardi, M.T. Farmer, D.J. Kilsdonk, J.J. Sienicki, and C. Grandy, "Fundamental Na-CO_2 Interactions in Compact Heat Exchangers Experiment (SNAKE): Fiscal Year 2011 Status Update," ANL-ARC-199, (2011).
6. C. Gerardi, M.T. Farmer, D.J. Kilsdonk, J.J. Sienicki, and C. Grandy, "Na-CO_2 Interactions Experiment (SNAKE): Fiscal Year 2012 Update on Facility Assembly and Sodium Loading," ANL-ARC-230, (2012a).
7. C. Gerardi, M.T. Farmer, D.J. Kilsdonk, R. Aeschlimann, J.J. Sienicki, and C. Grandy, "Report on the Initial Fundamental Sodium-CO_2 Interaction Experiment," ANL-ARC-251, (2012b).
8. C. Gerardi, J.J. Sienicki, A. Moisseytsev, M.T. Farmer, and C. Grandy, "Test Matrix for the Fundamental Sodium-CO_2 Interaction Experiment (SNAKE)," ANL-SMR-2, (2013).
9. L. Gicquel, C. Latgé, and N. Simon, "Supercritical CO_2 Brayton Cycle Coupled with a Sodium Fast Reactor: Na/CO_2 Interaction Experiments and Modeling," Paper 10215, 2010 International Congress on Advances in Nuclear Power Plants (ICAPP '10), San Diego, CA, USA, June 13-17, (2010).
10. L. Gicquel, C. Latgé, and N. Simon, Ph. Hobbes, A. Soboni, J.C. Buvat, J.L. Gustin, "Brayton Cycle with SC-CO_2: Investigations of Sodium-Carbon Dioxide Interactions," Slides from Meeting with A. Moisseytsev (ANL), April 27-29, (2011).
11. D. Gifford, S. Kreger, A. Sang, M. Froggatt, R. Duncan, M. Wolfe, B. Soller, "Swept-wavelength interferometric interrogation of fiber Rayleigh scatter for distributed sensing." Proc SPIE 6770 Fiber Optic Sens and Appl V 67700F, (2007).
12. *Liquid-Metals Handbook*, US Office of Naval Research, (1950).

13. S. Lomperski, C. Gerardi, W.D. Pointer, "Distributed fiber optic temperature sensing for CFD code validation." Proceedings of 15th International Topical Meeting on Nuclear Reactor Thermal Hydraulics (NURETH-15) Pisa, Italy, (2013).
14. S. Lomperski, C. Gerardi, "Assessment of distributed fiber optic sensors for flow field temperature mapping." Proc. ASME 2014 4th Joint US-European Fluids Engineering Division Summer Meeting (2014).
15. S. Lomperski, C. Gerardi, W.D. Pointer, "Fiber Optic Distributed Temperature Sensor Mapping of a Jet-Mixing Flow Field," Experiments in Fluids (submitted; 2014).
16. MSA Infrared Gas Monitor Instruction Manual, Rev 3, (2006).
17. NIST Thermophysical Properties of Fluid Systems, http://webbook.nist.gov/chemistry/fluid/, Accessed April (2013).
18. Z. Renjun, J. Xinzhen, L. Baozhang, Z. Yong, and Z. Laiqi, "Studies on Gas Holdup in a Bubble Column Operated at Elevated Temperatures," Ind. Eng. Chem. Res, Vol. 27, pp. 1910-1916, (1988).
19. A. Sang, M. Froggatt, D. Gifford, S. Kreger, B. Dickerson, "One Centimetre Spatial Resolution Temperature Measurements in a Nuclear Reactor using Rayleigh Scatter in Optical Fiber." IEEE Sensors J 8(7):1375-1380, (2008).
20. S.R. Sherman, S.P. Henslee, K.E. Rosenberg,, C.J. Knight, K.J. Belcher, D.E. Preuss, D.H. Cho, C. Grandy, "Unique Process for Deactivation of Residual Sodium in LMFBR Systems," Proceedings of Spectrum 2002, American Nuclear Society, Reno, Nevada, U.S.A., August 4-8, (2002).
21. *Sodium Technology*, Atomics International: North American Rockwell, (1970).
22. R. Span, and W. Wagner, "A New Equation of State for Carbon Dioxide Covering the Fluid Region from the Triple-Point Temperature to 1100K at Pressure up to 800 MPa," J. Phys. Chem Ref. Data, Vol. 25(6), pp. 1509-1596, (1996).
23. N.E. Todreas, and M.S. Kazimi, *Nuclear Systems I: Thermal Hydraulic Fundamentals*, Taylor & Francis, (1990).

Argonne
NATIONAL LABORATORY

Nuclear Engineering Division
Argonne National Laboratory
9700 South Cass Avenue
Argonne, IL 60439

www.anl.gov

Argonne National Laboratory is a U.S. Department of Energy laboratory managed by UChicago Argonne, LLC